Neuron
Article

Coherent Theta Oscillations and Reorganization of Spike Timing in the Hippocampal-Prefrontal Network upon Learning

Karim Benchenane,[1,7,*] Adrien Peyrache,[1] Mehdi Khamassi,[1,2] Patrick L. Tierney,[3,4] Yves Gioanni,[3] Francesco P. Battaglia,[1,5,6,*] and Sidney I. Wiener[1,6]
[1]Laboratoire de Physiologie de la Perception et de l'Action, Collège de France, CNRS, 11 place Marcelin Berthelot, 75231 Paris CEDEX 05, France
[2]Institut des Systèmes Intelligents et de Robotique, Université Pierre et Marie Curie – Paris 6, CNRS FRE 2507, 4 Place Jussieu, 75252 Paris Cedex, France
[3]INSERM U667, Collège de France, 11 place Marcelin Berthelot, 75231 Paris CEDEX 05, France
[4]Massachusetts Institute of Technology, McGovern Institute for Brain Research, Cambridge, MA 02139 USA
[5]SILS Center for Neuroscience, Universiteit van Amsterdam, Science Park 904, 1098XH Amsterdam, The Netherlands
[6]These authors contributed equally to this work
[7]Present address: ENMVI team, CNRS UMR 7102, Université Pierre et Marie Curie, Quai Saint-Bernard 75005 Paris, France
*Correspondence: karim.benchenane@snv.jussieu.fr (K.B.), f.p.battaglia@uva.nl (F.P.B.)
DOI 10.1016/j.neuron.2010.05.013

SUMMARY

To study the interplay between hippocampus and medial prefrontal cortex (Pfc) and its importance for learning and memory consolidation, we measured the coherence in theta oscillations between these two structures in rats learning new rules on a Y maze. Coherence peaked at the choice point, most strongly after task rule acquisition. Simultaneously, Pfc pyramidal neurons reorganized their phase, concentrating at hippocampal theta trough, and synchronous cell assemblies emerged. This synchronous state may result from increased inhibition exerted by interneurons on pyramidal cells, as measured by cross-correlation, and could be modulated by dopamine: we found similar hippocampal-Pfc theta coherence increases and neuronal phase shifts following local administration of dopamine in Pfc of anesthetized rats. Pfc cell assemblies emerging during high coherence were preferentially replayed during subsequent sleep, concurrent with hippocampal sharp waves. Thus, hippocampal/prefrontal coherence could lead to synchronization of reward predicting activity in prefrontal networks, tagging it for subsequent memory consolidation.

INTRODUCTION

Selective communication between brain areas is a key component of the neural processing underlying cognition. This information exchange must adapt to the current situation and brain state, with functional networks continuously forming and disbanding (Fell et al., 2001). This would help filter and select signals to be processed and transmitted to other areas, possibly supported by the emergence of highly synchronized activations of cell groups or cell assemblies representing a highly effective input for afferent structures (Hebb, 1949; Fries, 2005; Fries et al., 2007). The resulting dialog would drive plastic changes in short- and long-range synaptic connections and contribute to create widespread integrated representations of items and experiences, selecting and retaining the information most valuable for adaptive behavior. Such valence and salience information is thought to be transmitted by neuromodulators such as dopamine, which could act as a reward prediction (error) signal (Schultz et al., 1997; Dayan and Balleine, 2002; Doya, 2008).

Brain rhythms are likely to be a fundamental mechanism for modulating, filtering, and redirecting information in the nervous system: neural circuits are naturally predisposed to oscillate in a wide range of frequencies (Buzsáki, 2004). Oscillations are a key mechanism of dynamical coupling between brain areas: task- and state-dependent changes are observed in local field potential (LFP) coherence (Fell et al., 2001; Varela et al., 2001; Womelsdorf et al., 2007) and in cross-correlated unit activity (Tabuchi et al., 2000; Engel et al., 2001). From the functional point of view, synchronizing and desynchronizing activity between two brain areas exert dramatic effects on their ability to engage or effectively block out one another's input (Womelsdorf et al., 2007). Within individual brain areas, oscillations can synchronize neurons, creating coherent cell assemblies (Harris et al., 2003) and favoring plasticity processes depending on the precise timing of pre- and postsynaptic activity (Markram et al., 1997; Bi and Poo, 1998; Cassenaer and Laurent, 2007). However, little is known about the mechanisms underlying such synchronization-induced modifications of local functional circuitry. Here, we will examine learning-related changes in oscillatory coherence between hippocampus and Pfc and associated changes in Pfc local circuitry, which will be shown to closely resemble the effects of local application of dopamine.

The hippocampus-neocortex network is a primary conduit for cerebral information flow for learning and memory. Anatomically

located at the top of the cortical hierarchy (Felleman and Van Essen, 1991), the hippocampus (Hpc) was proposed to create "pointer" representations, linking together activity in multiple cortical areas pertaining to the same context and facilitating the formation of permanent cortical episodic memory traces (Eichenbaum, 2000; Shastri, 2002; Moscovitch et al., 2005; Frankland and Bontempi, 2005). Effective communication between the hippocampus and the neocortex involves oscillations: for example, transient synchronization at gamma (30-80 Hz) frequencies between the Hpc and the rhinal cortex accompanies successful memory encoding (Fell et al., 2001). Pfc, which receives monosynaptic hippocampal projections (Jay and Witter, 1991; Thierry et al., 2000), has been shown to be functionally connected to the hippocampus: Hpc theta (5–10 Hz) synchronizes medial prefrontal cortex (Pfc) neurons (Siapas et al., 2005) and LFPs (Hyman et al., 2005) depending on task demands (Jones and Wilson, 2005), possibly supporting corticohippocampal maintenance of working memory (Floresco et al., 1997).

This study examines changes in synchronization of Hpc and Pfc LFPs and single and ensemble Pfc neuron activity in rats learning and flexibly switching between rules. If oscillatory coherence plays a role in memory encoding and acquisition, it would be expected to vary with learning, and to be associated with the creation of neural substrates of memories, possibly in the form of functionally linked cell assemblies (Hebb, 1949). If those cell assemblies carry relevant information, then they should be more readily consolidated into long-term memory (Peyrache et al., 2009b).

These hypotheses are examined here. However, the mechanism by which these assemblies would be "tagged" at acquisition is not known, and evidence will be put forward for this in the form of coherence-induced and (possibly dopamine influenced) creation of learning-related, reward-predictive cell assemblies that are tightly synchronized, permitting their stabilization by spike-time dependent plasticity.

RESULTS

Hpc-Pfc Theta Coherence

We recorded a total of 1475 Pfc neurons (see Figure S1 available online) in 60 experimental sessions in four rats as they successively learned two reward contingency rules on a Y maze: go to the arm on the right and then go to the lit arm (selected at random at each trial; Figures S2A and S2B). LFPs were recorded in the pyramidal layer of ventral/intermediate hippocampal CA1, while multielectrode single-unit spike activity and LFPs were recorded in medial Pfc (Figure S1A–S1D). Strong 5–10 Hz theta band LFP activity was detectible in both Hpc and Pfc (Jones and Wilson, 2005; Hyman et al., 2005; Figures 1A and 1B). Strong Hpc-Pfc spectral coherence was observed in the theta frequency range (Figures 1A and 1B). Hpc-Pfc-θ-coherence fluctuated, with no simple relation with either theta power in the two structures or with rat motion (Figures 1A and S2). On a trial-by-trial basis, coherence at the decision point did not correlate with running speed ($r = 0.04$, $p > 0.05$), which correlates with Hpc theta amplitude (Ekstrom et al., 2001) or with acceleration ($r = 0.01$, $p > 0.05$; see Figure S2). The phase lag between Hpc and Pfc theta rhythm was 40 ± 4 ms, similar to previous reports (Jones and Wilson, 2005) and compatible with Pfc response latencies to stimulation of the Hpc (Dégenètais et al., 2003). Thus, while the mechanism underlying this coherence is not known, it would nonetheless dramatically augment prefrontal receptivity to hippocampal signals.

To control for potential contamination of LFP coherence measures by volume conduction artifacts (Sirota et al., 2008), we compared LFP-LFP coherence with LFP-spikes coherence in the same structures (Womelsdorf et al., 2007) (Figures 1B, 1C, S1E and S1F). Of the 1373 Pfc neurons with average firing rates exceeding 0.01 Hz, 541 (39%) were significantly modulated by Hpc theta ($p < 0.05$, Rayleigh test). Coherence of Pfc spikes to Hpc LFP is most marked in the theta range (Figures 1B and 1C). Moreover, the time courses of coherence of prefrontal LFP and spike trains with hippocampal LFP show peak correlations in the theta frequency range, both for single prefrontal units (Figures 1B and 1C) and when all theta-modulated cells in a session are considered (Figures S1E and S1F). In the latter case, the correlation reached significance in the theta range only (Figure S1F). Thus, local Pfc circuits are likely to be involved in the expression of coherence with Hpc theta both at the LFP and spike train levels.

Hpc-Pfc-θ-Coherence Increases at the Maze Choice Point, Particularly upon Learning

Coherence peaked when the rat was at the fork of the Y maze (Figures 2A and 2B). Strikingly, the increase of coherence at the choice point was significantly greater after acquisition of a new rule (Figures 2C–2E; *Right*, n = 123; *Light*, n = 148, two-way ANOVA, factors: before/after learning (L) and position on maze (P); *Right*, main effects: L: $p < 0.01$, P: $p < 10^{-5}$, interaction $p < 0.02$; *Light*, main effects L: $p < 10^{-4}$, P: $p < 10^{-5}$, interaction $p < 0.01$). This effect was observed for LFPs recorded in both superficial and deep layers of Pfc (Figure S2C). Similarly, Hpc-Pfc-θ-coherence at the choice point was higher at a learning stage when the rat reliably complied with the rewarded rule (compared with trials prior to criterion performance; Figure 2F, t test, $p < 0.05$), as assessed by high values of the "certainty" measure developed by Smith et al. (2004). This was not merely due to the higher incidence of rewards after rule acquisition, since, when considering only trials prior to this, coherence was not significantly different between rewarded and unrewarded trials (Figure 2G; n = 271, t test, $p > 0.05$). These results, taken together, suggest that Hpc-Pfc-θ-coherence is a predictor of the rat's performance level: indeed, we show that trials with high coherence had, on average, a high level of performance, whereas in trials with low decision point coherence, rats operated at only slightly better than chance level (Figure 2H).

Increased Correlations between Pfc Cell Pairs during High Hpc-Pfc-θ Coherence

Because coherence was elevated upon learning and functional connectivity in the Pfc network increases with learning (Baeg et al., 2007), we tested for changes in activity correlations in simultaneously recorded prefrontal neurons during high Hpc-Pfc-θ coherence episodes. During high coherence periods the distribution of correlation coefficients between all

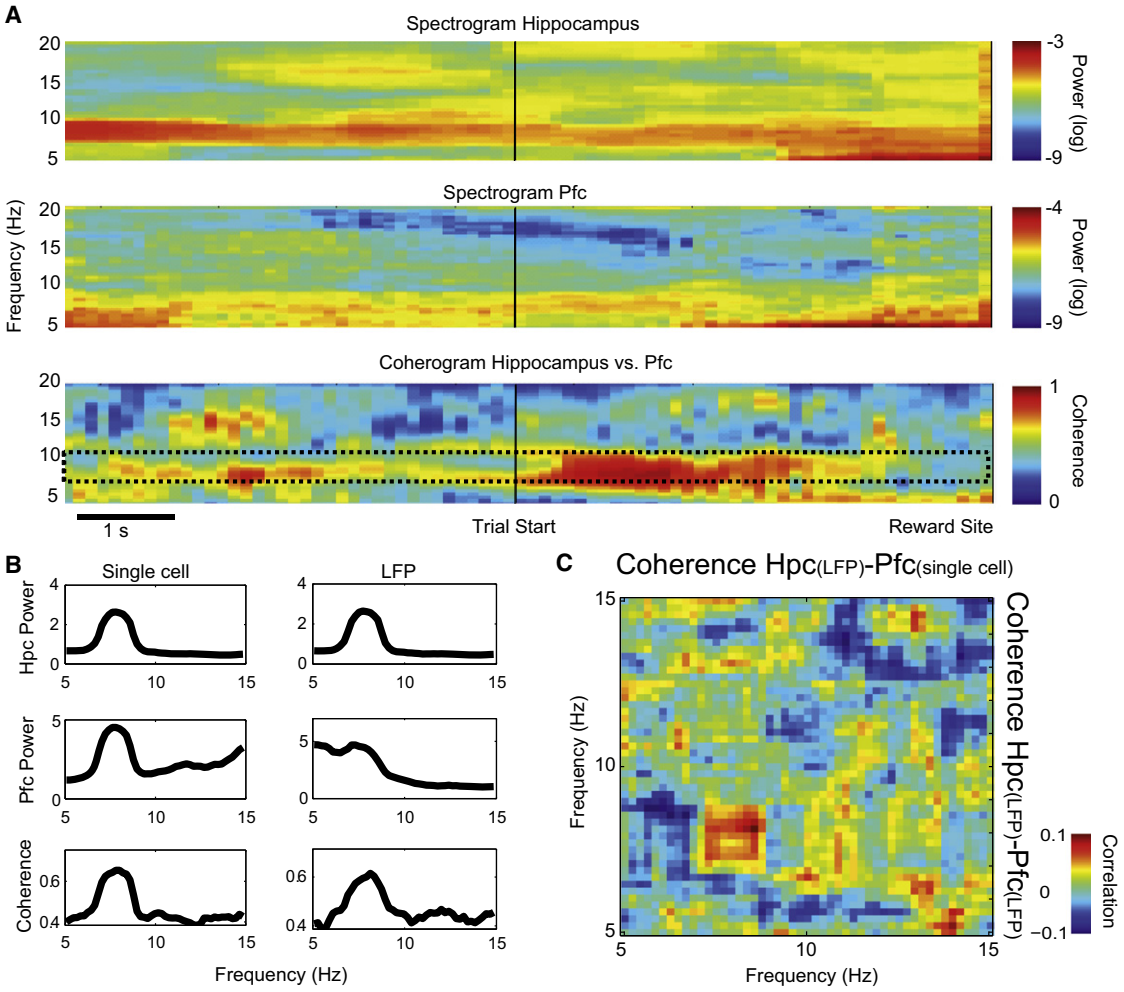

Figure 1. Characterization of Hpc-Pfc Theta Coherence

(A) Spectrograms of Hpc and Pfc LFPs and Hpc-Pfc coherence during a representative trial. Theta band coherence peaks at the maze choice point, where hippocampal and prefrontal theta amplitudes are not maximal.

(B) Top and middle, power spectra of Hpc and Pfc LFP (right) and Hpc LFP and a representative Pfc neuron's instantaneous firing rate (left). Bottom, coherence spectra between Hpc and Pfc LFP (right) and between Hpc LFP and a single Pfc neuron's instantaneous firing rate (left).

(C) Correlation between the time series for Hpc-Pfc LFP spectral coherence (ordinate) and the coherence between Hpc LFP and spikes of a single Pfc neuron (abscissa) as a function of frequency.

See also Figure S1.

simultaneously recorded neurons pairs shifted relative to low coherence periods (Figure 3A, Kolmogorov-Smirnov-test, $p < 0.05$ each day). During high coherence, cell pairs with elevated correlation values appeared (Figure S3A). This reveals a profound modification in the dynamics of the prefrontal neuronal network when Hpc-Pfc-θ coherence is high.

Preferential Participation of Hpc Theta Modulated Pfc Neurons in Cell Assemblies Formed upon Learning

The increase in significant correlations in cell pairs during high (versus low) Hpc-Pfc-θ coherence periods was restricted to those Pfc neurons modulated by Hpc theta (Figure 3B; $n = 32$, two-way ANOVA with factors theta modulation and high/low coherence: effect of interaction $p < 0.05$ and post hoc t test, $p < 0.01$). In contrast, pairs of neurons with one or both not modulated by Hpc theta showed no significant change in coactivation during high coherence periods (Figure 3B). In the five sessions with new rule acquisition (and at least 20 simultaneously recorded neurons), only after rule acquisition, but not before, were pairs of theta-modulated neurons more likely to be significantly correlated than pairs of neurons without theta modulation (Figures 3C and S3; $n = 5$ two-way ANOVA with factors high/low coherence and before/after learning and post-hoc t test, $p < 0.05$). Thus, rule acquisition corresponded to increased coactivation within subpopulations of Hpc modulated Pfc neurons. The increased activity correlations held at two time scales, whether firing rates were binned at 30 ms or by theta cycle (approximately 125 ms) time windows (Figure S3). This

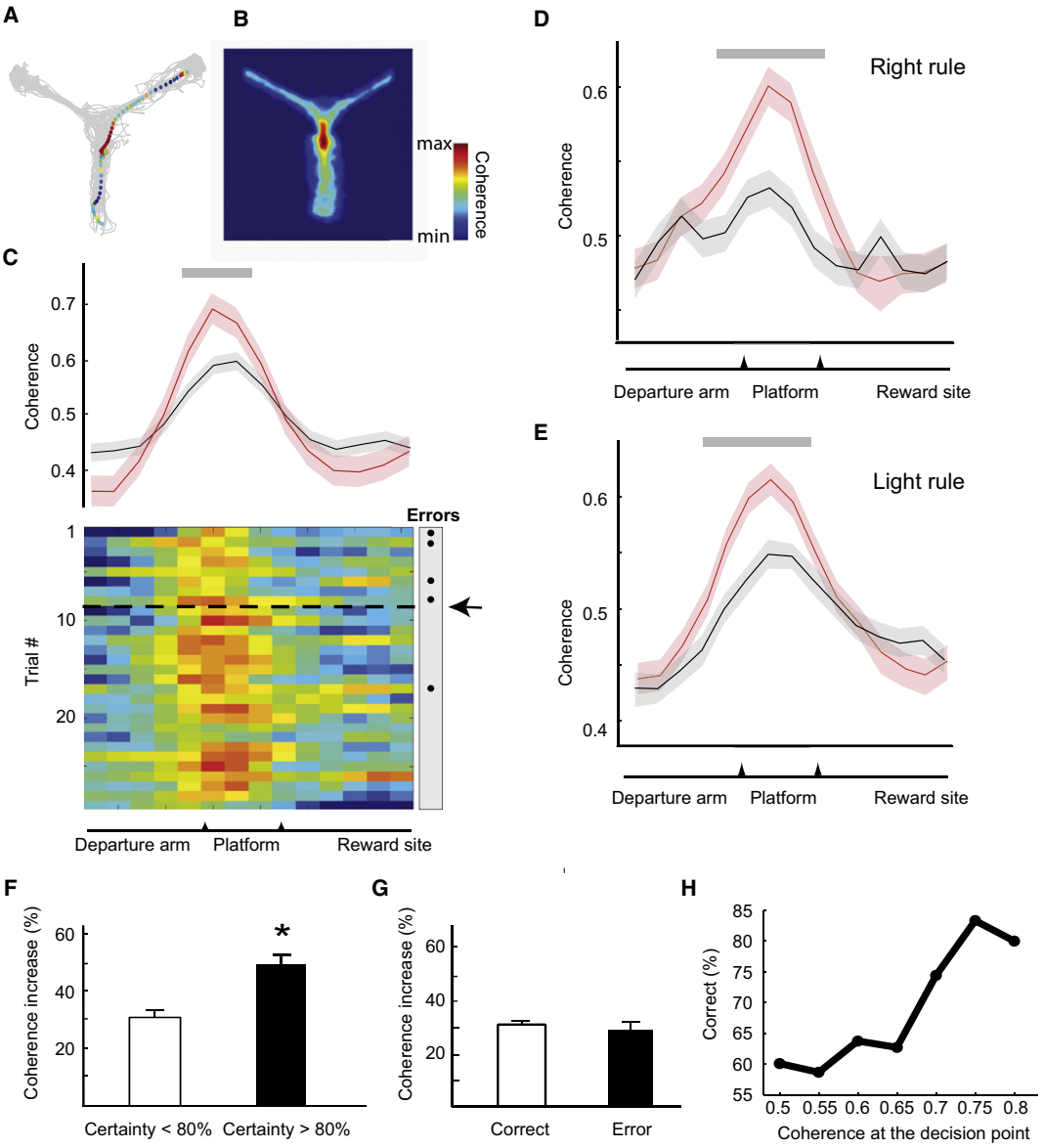

Figure 2. Coherence Increases at the Choice Point upon Learning

(A) Instantaneous Hpc-Pfc theta coherence (color coded) for one trial (overhead view). Each color point represents the average value over a 100 ms sample. Note that high coherence values appeared as the rat started to veer toward the chosen arm. Gray background traces correspond to the rat's trajectories for the rest of the session. Scale bar: min = 0, max = 0.9.

(B) "Coherence map:" average Hpc-Pfc theta coherence recorded at each point on the maze. Data is averaged over all sessions. Scale bar: min = 0, max = 0.6.

(C) Hpc-Pfc theta coherence increases upon learning. Top, mean coherence for positions along the maze before (black) and after rule acquisition (red) for one session. Coherence increases at the decision point after rule acquisition. Bottom, color raster plot of Hpc-Pfc theta coherence as a function of position on the maze for each trial before and after learning (horizontal dashed bar, at right black dots indicate error trials) in the same session. Gray bar above (C), (D), and (E): significant effect of learning, $p < 0.05$ (two-way ANOVA followed by post hoc t tests).

(D and E) Mean Hpc-Pfc theta coherence in all the sessions in which rats learned (D) the Right rule (n = 123 trials before and after rule acquisition, over 9 sessions, 4 rats), and (E) the Light rule (n = 148 trials before and after rule acquisition, over 12 sessions, 4 rats).

(F) Increase in Hpc-Pfc theta coherence at the choice point compared to baseline (defined by averaging coherence during the first three and last five bins for the histograms of Figure 2D) in trials with high versus low certainty (Smith et al., 2004) values (high: n = 196, low: n = 346, t test, $p < 0.05$).

(G) Comparison of Hpc-Pfc theta coherence at the choice point in rewarded versus unrewarded trials before rule acquisition (rewarded: n = 131, unrewarded: n = 140, t test, $p > 0.05$).

(H) Relation between decision point coherence and performance. Ordinate is the percentage of correct responses for all trials whose coherence at the decision point exceeds the abscissa value.

See also Figure S2.

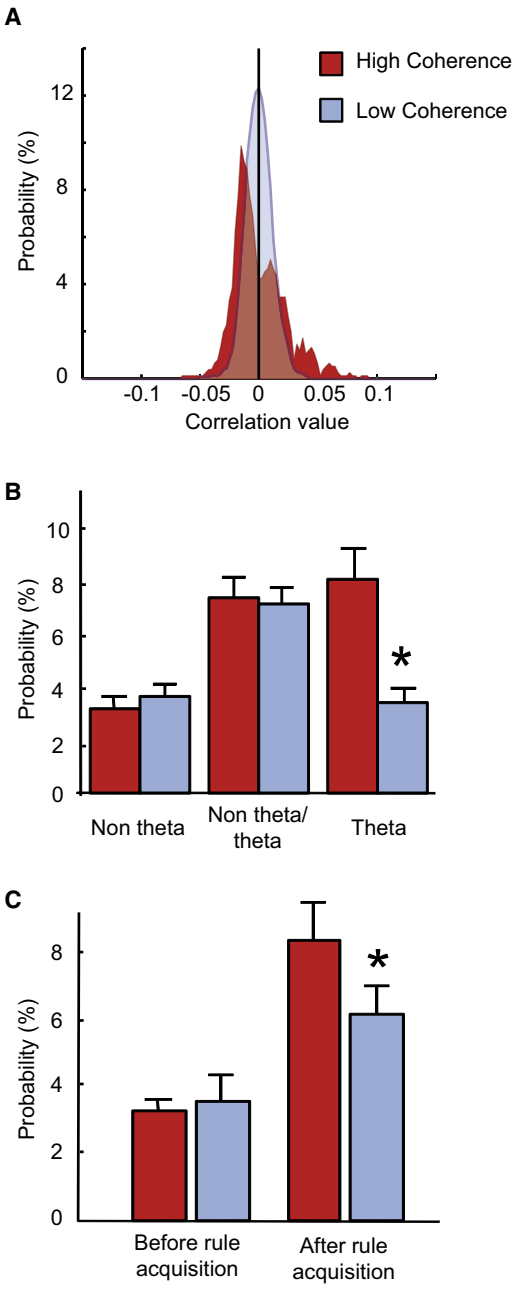

Figure 3. Modification of Pfc Functional Circuitry during High Coherence Periods

(A) Distribution of correlation coefficients for all simultaneously recorded neuron pairs in a single representative session. Binned spike trains (bin size: 30 ms) were taken from high (red filled area) or low coherence periods (blue filled area). (The distributions are significantly different, Kolmogorov-Smirnov-test, $p < 0.05$.)

(B) Proportion of pairs of neurons with significant correlations among (from left to right) all pairs of non-theta modulated cells, among pairs consisting of a theta-modulated and a non-modulated cell, or pairs of theta-modulated cells, computed for high and low theta coherence periods. The incidence of pairs of theta modulated neurons increased during high coherence epochs ($n = 32$ sessions, t test, $p < 0.01$; number of neurons recorded simultaneously in those sessions: min: 7, max: 55; same color code as in *A*).

(C) Same analysis as (B) in sessions with rule acquisition, divided into trials before and after rule acquisition, for theta-modulated cell pairs only. Same color code as in (A); $n = 5$ sessions, two-way ANOVA, post hoc t test, $p < 0.05$). See also Figure S3.

indicates that, during high coherence periods, theta modulated cell pairs tend to fire together within the same theta cycle, as well as at a shorter time scale.

Pfc Cell Assemblies Are Formed during High Coherence Periods

The network reorganization during high Hpc-Pfc-θ-coherence suggested by the results in Figure 3 may reflect not just coactive pairs of neurons, but rather synchronization of activity in subgroups of neurons, or cell assemblies, as proposed by Hebb (1949). Neuronal groups that coactivate reliably and hence act as cell assemblies can be extracted by principal component analysis (PCA) applied to the matrix of binned simultaneously recorded spike trains (Chapin and Nicolelis, 1999; Cassenaer and Laurent, 2007; Peyrache et al., 2009a, 2009b), and the time course of their activation can be calculated from the principal component (PC) scores of the instantaneous population vectors (see Experimental Procedures; Peyrache et al., 2009a, 2009b).

Since pairwise correlations increased during high Hpc-Pfc-θ coherence periods, PCA was applied to 30 ms bins of spike trains of units simultaneously recorded then, and the strongest components were retained (see Experimental Procedures). The signs of the coefficients of each PC distinguished two neuronal populations: cells with high weights and same sign coefficients which fire together, and cells with high weights but opposite signs which are anti-correlated (Figure S4A). Thus, the projection of the recorded coactivation onto the PC at each time bin describes the temporal evolution of the activation of the neuronal assembly (Peyrache et al., 2009a; Figure S4A and S4B). Figure 4A shows examples of time courses of PC activations (see Experimental Procedures), showing high, transient peaks occurring over a very low background. These peaks correspond to the coordinated activation of those cells with elevated, positive weights in the PC (displayed in the upper rasters), and occurred during periods of high Hpc-Pfc-θ-coherence. The transient nature of PC activation time courses (Peyrache et al., 2009a) was observed throughout the recordings as shown by the elevated tail (relative to power law decay) of the histogram of activation values over time. (Figure S4C and S4D). We therefore termed these strong bouts of coactivation (Figures 4A, S4A, and S4B) coherence-related cell assemblies (CRCA). Here, we considered the cells with the five largest coefficients in the PC as taking part in the CRCA, defined as the times in which the PC activation measure exceeded a threshold value of 3 (Figures S4C and S4D). Results did not change when different values of the threshold were considered (Figure S4E).

CRCA frequency increased in elevated Hpc-Pfc-θ-coherence periods relative to low coherence periods (paired t test $p < 10^{-200}$; Figure 4B). Similarly to coherence (Figures 2A and 2B), their spatial distribution presented a distinctive peak at the decision point (Figure 4C).

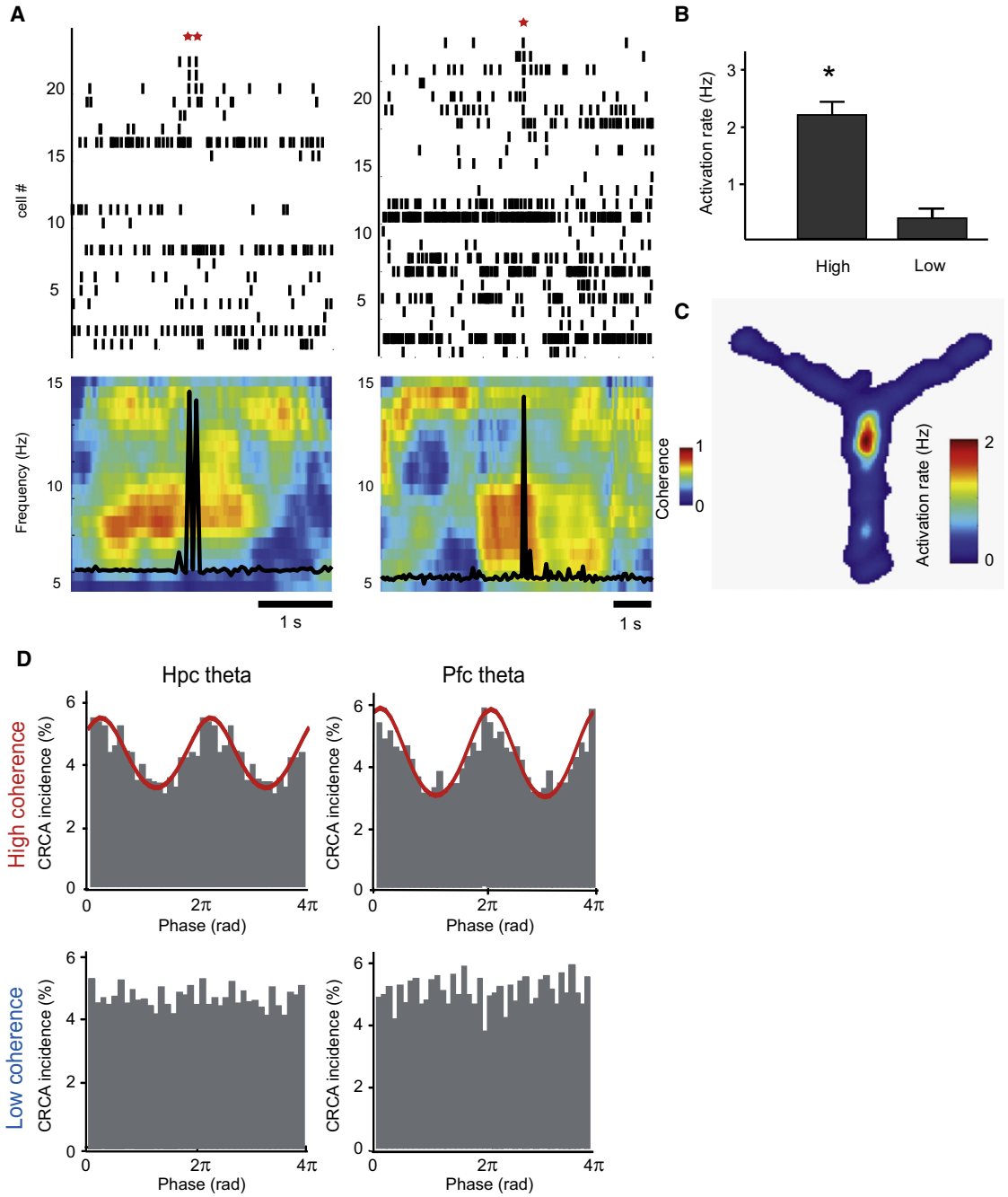

Figure 4. Identification of Theta Coherence-Related Cell Assemblies (CRCA)

(A) Above, raster displays of simultaneously recorded neurons ordered from top to bottom according to their contributions to the cell assembly (PC weights) in two recording sessions. Below, temporal evolution of instantaneous subnetwork coactivation computed as in Peyrache et al. (2009b) (black trace) is superimposed on the concurrent LFP Hpc-Pfc coherence spectrograms. Note that peaks in PC score correspond to synchronization of neurons with high PC weights (neurons 19–23 on the left, neurons 21–27 on the right; red stars above). These peaks occur during periods of high LFP theta coherence.

(B) Mean activation rate of CRCA during high versus low coherence periods (n = 92, paired t test, $p < 10^{-200}$).

(C) Spatial distribution of the peaks in the subnetwork coactivation corresponding to the CRCAs computed for 35 sessions. Note the concentration at the maze choice point.

(D) Phase of CRCA relative to hippocampal theta (left) or prefrontal theta (right) during high or low coherence periods. Modulation is highly significant for high coherence periods for Hpc theta phase (n = 92 from 35 sessions, upper left, $\kappa = 0.26$, Rayleigh Z test, $p < 10^{-26}$, $\phi_{pref} = 0.71$) and Pfc theta phase (n = 92 from 35 sessions, upper right, $\kappa = 0.33$, Rayleigh Z test, $p < 10^{-31}$, $\phi_{pref} = 0.34$), but not for low coherence periods (n = 92, Rayleigh Z test, $p > 0.05$). (See Figures S4 and S5 for control analyses.)

During High Coherence Periods Pfc Cell Assemblies Are Phase-Locked to the Trough of Hippocampal Theta

We analyzed the phase locking of Pfc CRCA activity to the hippocampal theta rhythm. For each recording session, at least one of the PCs identified a Pfc cell assembly significantly modulated by Hpc theta (i.e., with a significant Rayleigh Z test, $p < 0.05$). Notably, during high coherence periods, the phases of occurrence of these Pfc CRCAs were concentrated at the trough of theta recorded in both Hpc CA1 stratum pyramidale and in Pfc ($n = 92$, Rayleigh Z test, $p < 10^{-26}$), that is, the theta phase at which hippocampal CA1 cell assemblies are principally active (Harris et al., 2003). On the other hand, during low coherence periods, the theta phase of CRCA occurrence was uniformly distributed (Figure 4D). The same result was obtained when PCA extracted assemblies from spike trains grouped by theta cycle (~125 ms time bins; Figure S5A). This rules out the possibility that these observations could be an artifact due to PCA merely capturing subsets of neurons with similar theta modulation. Moreover, this increased phase locking in high coherence periods was not observed in the general neuronal population. Rather, it was limited to those cell assemblies more strongly active during high coherence periods, because no such effects were observed in PCs with low signal strengths, likely corresponding to 'noise' (Peyrache et al., 2009a, 2009b; $p > 0.05$, $n = 70$) or for PCs computed from low coherence periods ($p > 0.05$, $n = 72$; Figure S5B). Thus, high Hpc-Pfc-θ-coherence signaled a state in which Hpc and Pfc assemblies are aligned at the same theta phase, possibly favoring interaction.

Local Circuit Dynamical Changes Possibly Underlying Assembly Formation

To investigate the neurophysiological processes leading to the formation of CRCA, we analyzed the behavior of the cells with the five largest weight coefficients in the PC (positive and negative), that is, the ones most likely to participate in synchronous firing events. These neurons were then subdivided according to their putative cell type on the basis of action potential duration (Barthó et al., 2004; Figure S6A).

Interneurons play a specific and crucial role in the generation and maintenance of theta and other brain rhythms (Buzsáki, 2002; Klausberger et al., 2003). Furthermore, prefrontal interneurons are directly innervated by hippocampal afferents (Tierney et al., 2004). Thus, we analyzed the theta phase locking behaviors of 234 Pfc theta modulated interneurons and pyramidal cells with high absolute PC weights in the CRCAs. Among neurons forming the cell assemblies, 189 putative pyramidal neurons (81%) and 34 (15%) interneurons were identified (Figures 5A–5D). The preferred phases of putative interneurons were concentrated at the peak of theta in periods of both high and low coherence (Figure 5B; $n = 34$, $p < 0.005$), and showed no coherence-dependent changes in Hpc theta modulation strength kappa (Figure 5D; $n = 34$, paired t test, $p > 0.05$).

In contrast, in putative pyramidal cells, as LFP Hpc-Pfc-θ coherence increased, the strength of theta modulation also augmented (Figure 5D; $n = 189$, t test, $p < 0.05$). Moreover, putative pyramidal neurons active in cell assemblies selectively changed their phase preference in a particular fashion: those neurons phase-locked with the Hpc θ peak (at π) during low coherence shifted their phase preference to 2π to match the phase of the CRCA during high coherence. Indeed, preferred phases of pyramidal neurons and CRCA (Figure 4D) are not significantly different during high coherence periods, ($n = 189$, $n = 92$, circular ANOVA, $p > 0.05$). On the other hand, those Pfc neurons whose preferred phase was already at the trough of Hpc θ (2π) during low coherence maintained this preferred phase within high-coherence CRCA events (Figure 5A, $n = 189$, $n = 34$, circular ANOVA, $p < 0.05$).

Interestingly, during high coherence, the preferred phases of pyramidal neurons converged on the preferred phase of the CRCA, in contrast with the interneurons (Figure 5C). Note that this is not due to possibly improved reliability of phase measurements resulting from an increase in hippocampal theta power during high coherence periods. Indeed, there is no significant difference in theta power during high and low coherence ($n = 21$, t test, $p > 0.05$; Figure 7E). Furthermore, Hpc theta power tended to be higher in low coherence periods beyond the fork of the maze, corresponding to when the rat ran faster.

Interneuron-Principal Neuron Inhibitory Efficacy Is Enhanced during High Coherence Periods

Behavior can strongly modulate inhibition in the Pfc (Constantinidis and Goldman-Rakic, 2002; Fujisawa et al., 2008) and, in turn, inhibition can exert a powerful influence on the firing phase of principal neurons relative to neuro-oscillatory activity (Chapman and Lacaille, 1999; Mann and Paulsen, 2007). Since putative principal and interneurons were differentially modulated by theta in high and low coherence periods, we hypothesized that periods of high and low Hpc-Pfc theta coherence would correspond to physiological states characterized by different inhibitory efficacies. Thus, we computed cross-correlograms between interneurons and pyramidal cells with high weights in PCs characterizing the CRCAs, with a method derived from Constantinidis and Goldman-Rakic (2002).

Putative interneurons effectively inhibited putative pyramidal cells during high coherence periods, but not during low coherence periods (Figure 5E for a single interneuron-pyramidal pair and Figure 5F for all interneurons analyzed, see Experimental Procedures): during high coherence periods, putative pyramidal cell firing was interrupted for 5–10 ms after putative interneuron spikes, ($n = 26$, paired t test between high and low coherence in the [0, 5 ms] time window, $p < 0.01$). No deviation from baseline was apparent during low coherence periods. This could have contributed to the principal neurons shifting their preferred phase to the trough of Hpc theta (in phase opposition to interneurons) and hence helped to synchronize the pyramidal neurons to fire in CRCAs. After rule acquisition this inhibition was selective for the decision point relative to other zones in the maze: putative interneurons significantly inhibited putative pyramidal cells in the first 5 ms after interneuronal discharge ($p < 0.05$). Such inhibition was not significant elsewhere on the maze, or anywhere on the maze before rule acquisition (Figure 5G; see Figure S6B for a cell-by-cell breakdown).

Dynamic Modification of the Preferred Phase of Pfc Neurons Forming the CRCA

As shown above, a subset of pyramidal neurons composing the CRCA changed their phase preference to match the phase of the

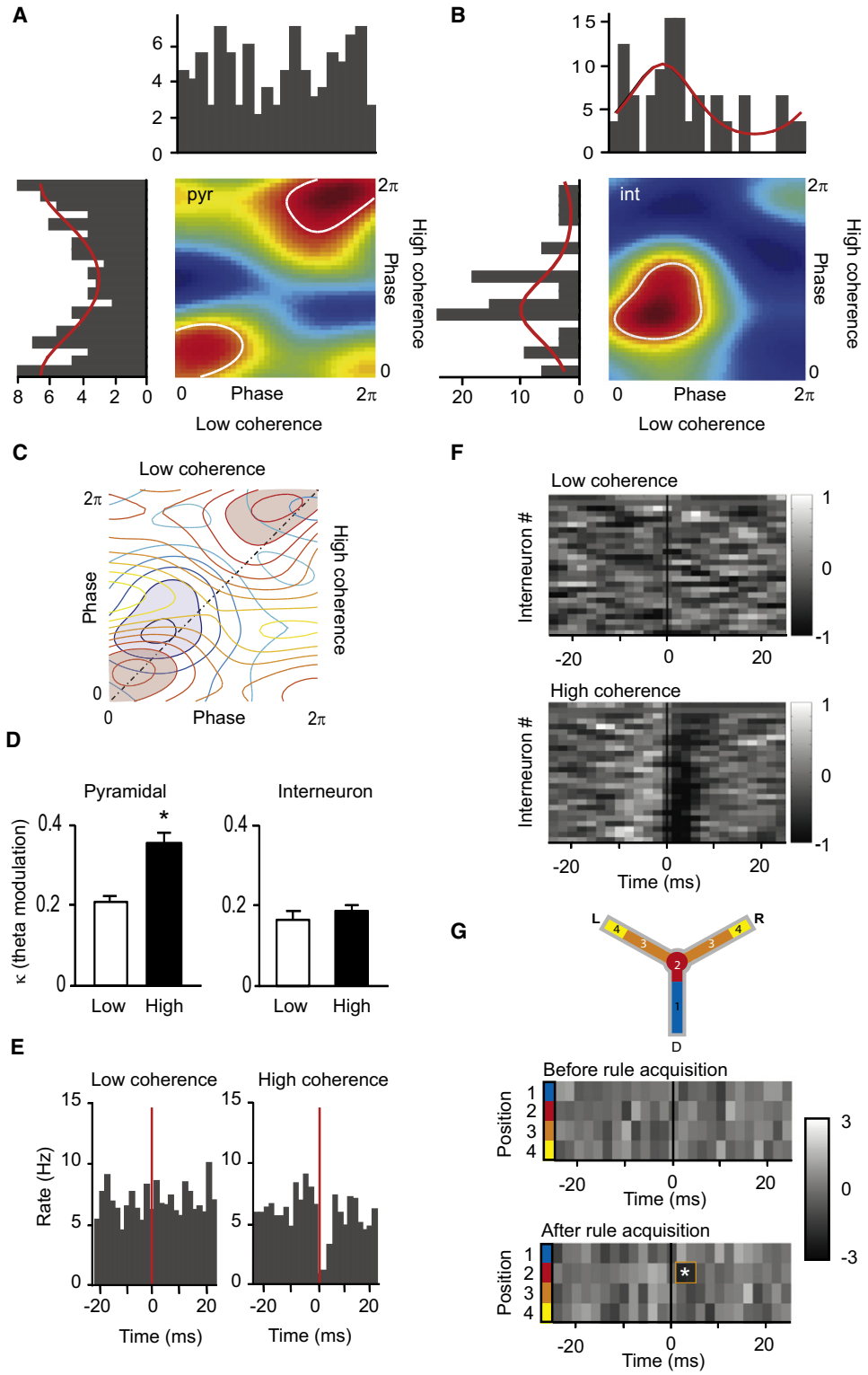

Figure 5. Pfc Interneurons and the Formation of Cell Assemblies

(A and B) Preferred Hpc theta phases of neurons with major contributions to cell assemblies (cells with the five highest and lowest weights in each session) during high (ordinate) or low (abscissa) coherence periods, considered separately as putative pyramidal cells (A, n = 189) and putative interneurons (B, n = 34). (A) Preferred phase plots of Pfc pyramidal neurons during high (ordinate) or low coherence periods (abscissa). The two-dimensional color histogram and its projections show that preferred phases did not deviate from a uniform distribution during low coherence periods (top, n = 189, κ = 0.13, Rayleigh Z test, p > 0.05),

CRCA during high coherence. In a representative example in Figure 6A, neuron 3 fired at the trough of Hpc theta continuously; on the other hand, neurons 2 and 4 fired at the peak of theta before the period of high coherence. During, the high coherence period, the firing phase of these two neurons shifted to the trough of theta. Neurons 1 and 5, previously silent, activated synchronously with the others in the CRCA. After the high coherence ended, the phase of neuron 4 returned to its previous value at the peak of theta. Hence, the neurons' phase shifts in Figure 5A can be seen as a dynamical process since this occurs progressively during the high coherence period. In this way phase realignment can effectively lead to synchronously activated cell assemblies.

In the same analysis of all pyramidal neurons forming the CRCAs, the phases of the spikes progressively shifted to the trough of theta leading up to activation of the CRCA (Figure 6B). Phase locking of these neurons was increased at the time of the CRCA as shown by the increased value of the concentration parameter κ, as computed by fit with a Von Mises distribution. However average firing rate did not change. This effect is directly related to CRCA since no modification of phase is seen when the reference is chosen at random times during high coherence periods (Figure S7).

Local Pfc Dopamine Application Also Increases Hpc-Pfc-θ Coherence and Reorganizes Neuronal θ Phase Preferences

Since the shifts in spike phases relative to theta and the consequent enhanced synchronization occurred at the decision point after rule acquisition, just as the rat reached an elevated level of certainty about the outcome of the current trial, we hypothesized that these local functional circuitry changes may be triggered by a reward prediction signal. Theoretical and experimental arguments (Schultz et al., 1997; Doya, 2008) suggest that this signal may be carried by a neuromodulator such as dopamine (DA). To test whether DA may induce similar effects on prefrontal neural activity, we recorded prefrontal single units and hippocampal LFPs in anesthetized rats (Figures 7C and S8), following locally iontophoretic application of DA in 1 min pulses. Figure 7A shows examples of spectrograms and a coherogram for Hpc and Pfc local field potentials, showing that, while theta power in the two structures remained constant, coherence increased after DA application (comparison of coherence readouts in 1 s time windows in the 3 min before and after DA application, t test, $n = 358$, $p < 0.05$; Figure 7B). This was also significantly different over all DA applications ($n = 20$, t test, $p < 0.05$; Figure 7F). Pyramidal cells and interneurons were classified based on spike width or marker labeling (Tierney et al., 2004). Interestingly, as observed during behavior for high Hpc-Pfc-θ coherence periods, pyramidal cells changed their theta phase locking, shifting from a preferred phase similar to those of interneurons before DA injection, to a phase opposite to interneuronal firing (circular ANOVA, $p < 0.05$; Figure 7D). Phase concentration for putative pyramidal cells increased as well ($n = 6$, t test, $p < 0.05$; Figure 7F). Similar to behavioral data for high Hpc-Pfc-θ-coherence, interneuron firing did not change theta phase ($n = 9$, t test, $p > 0.05$, Figure 7D–7F). The average phase change for putative pyramidal cells was significantly larger than that observed for interneurons (t test, $p < 0.01$; Figure 7F). Thus, a number of measures show a striking parallel between the effect of local Pfc DA, high coherence and phase shifts in the behaving animal (Figures 7E and 7F). Theta LFP coherence increased while power did not, pyramidal cells shifted and enhanced phase preference, while interneurons kept average firing preferences unchanged.

Enhanced Replay of CRCAs during Hippocampal Sharp Wave/Ripples

The memory consolidation theory holds that hippocampal traces are transmitted to cortical areas to build and reinforce long lasting traces. This would occur during sharp wave/ripple (SPWR) activity in slow-wave sleep (Girardeau et al., 2009; Peyrache et al., 2009b). A potential role for the high level of synchronization embodied by CRCAs is to favor synaptic plasticity so that cell assembly activation patterns can be successfully stored and reinstated. If this is the case, then the same cell assemblies would be expected to be more likely to activate spontaneously during the following slow-wave sleep. To test this, in data from slow wave sleep periods preceding

whereas they shifted to adopt a preferred phase ($\phi_{pref} = 6.2$ rad) relative to Hpc theta during high coherence periods (left, $n = 189$, $\kappa = 0.39$, Rayleigh Z test, $p < 0.0007$). Note that Pfc pyramidal neurons with preferred phases at the trough of Hpc θ during low coherence periods maintained this preferred phase within CRCAs, while those neurons firing at the Hpc θ peak during low coherence periods shifted to match the phase of the CRCA during high coherence. Red traces show best fits. White enclosure corresponds to top 10% values of the density distribution. (B) As in A but for Pfc putative interneurons. The preferred phases are concentrated at the peak of theta during both low ($n = 34$, $\kappa = 0.83$, Rayleigh Z test, $p < 0.005$, ϕpref = 1.76) and high coherence periods ($n = 34$, $\kappa = 0.90$, Rayleigh Z test, $p < 0.002$, ϕpref = 1.89); preferred phases of interneurons are not significantly different between high and low coherence periods ($n = 34$, circular ANOVA, $p > 0.05$).

(C) Superimposed contour plots from A and B for interneurons (shades of blue) and pyramidal neurons (shades of red and yellow). Shaded zones are the top 10% values of the density distribution.

(D) Strength κ of Hpc theta modulation of all Pfc putative pyramidal ($n = 189$) cells or interneurons ($n = 34$) with high PC weights during high and low coherence periods (t test, $p < 0.05$).

(E) Cross-correlograms of a putative interneuron (reference) and a putative pyramidal cell (both with high contributions to the cell assembly but with opposite signs) during high and low coherence periods. Note that the inhibition is clearly apparent in high, but not low, coherence periods.

(F) Cross-correlograms between simultaneously recorded interneuron and pyramidal cell pairs ($n = 26$) with high absolute PC weights show significantly greater inhibition during high coherence periods (paired t test in the [0, 5 ms] time window, $p < 0.01$, paired t test before [−5, 0 ms] and after [0, 5 ms], $p < 0.0001$). Gray scale shows normalized firing rate as z-scores.

(G) Top, four zones in the Y maze. Bottom, average cross-correlograms between simultaneously recorded interneuron and pyramidal cell pairs with high absolute PC weights in the four zones, before and after rule acquisition, showing significantly greater inhibition at the decision point after rule acquisition (paired t test before [−5, 0 ms] and after [0, 5 ms], *$p < 0.0001$). Gray scale shows normalized firing rates as z scores.

See also Figure S6.

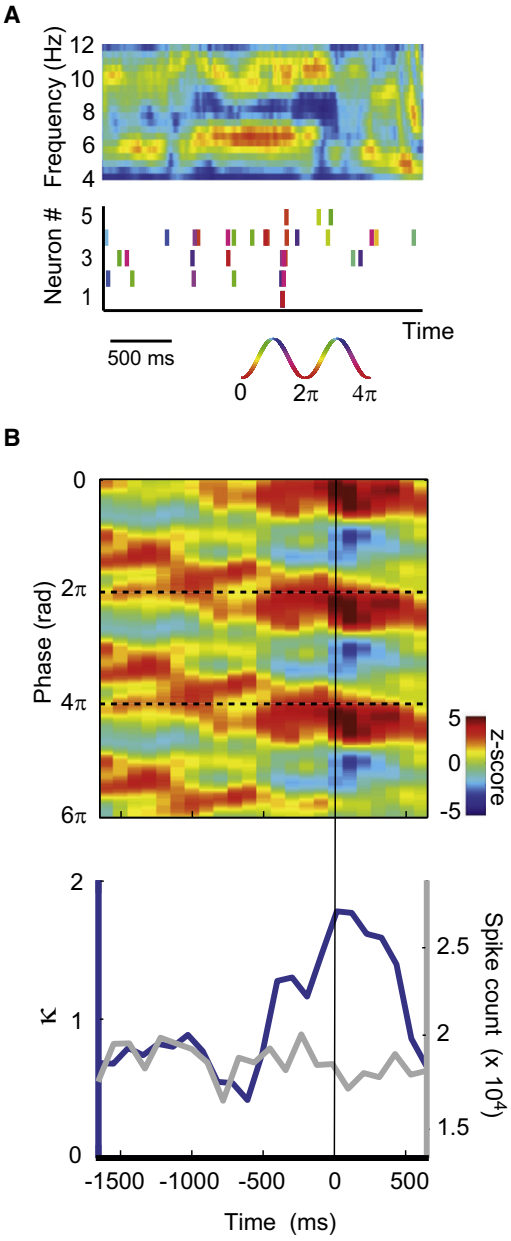

Figure 6. Formation of Cell Assemblies during High Theta Coherence Periods

(A) Top, a typical coherence spectrogram between Hpc and PfcLFPs. Bottom, raster display of neurons with highest positive weights in the CRCA. The phase of each spike with respect to Hpc theta is color coded as indicated below. Note that spikes' phases converge on the preferred phase of the assembly, so that the neurons discharge synchronously after several theta cycles at high coherence.

(B) Top, Distribution of spiking phases for neurons taking part in CRCA relative to CRCA activation (time zero). For each day with CRCA, histograms of spiking phase of all neurons forming the cell assemblies were computed according to their time relative to CRCA activation (100 ms bins). Histograms were normalized for each day and then averaged. Note the existence of two principal preferred phases: one remaining constant at the trough of theta (2π), the other beginning at the peak of theta and progressively shifting to its trough. Bottom, evolution of Kappa (blue) for the phase distributions in each 100 ms time bin. Gray trace shows the total number of spikes for each 100 ms time bin, demonstrating no overall modification of firing rate at the time of CRCA activation. Note the sharp upturn of Kappa several theta cycles (500 ms) prior to the CRCA activation.

See also Figure S7.

and following training sessions, we computed the reactivation strength (Peyrache et al., 2009b) for the PCs corresponding to CRCAs and event-triggered averages for the resulting time series, centered on SWPR. During sleep after the task, but not before, there was a significant increase in reactivation strength peaking 30–60 ms after SWPRs (t test, $n = 92$, $p < 0.01$; Figure 8). This was not the case for cell assemblies derived for low-coherence periods.

DISCUSSION

The principal findings here are (1) Hpc-Pfc theta coherence increases as the rat must determine the probability of future reward at the choice point in the maze, in particular after rule acquisition, when reward can be reliably predicted, (2) during elevated Hpc-Pfc theta coherence and upon new learning Hpc theta-modulated Pfc cells shift phase preference and assemblies form, and (3) local circuit properties reorganize in a manner which could underlie the formation of synchronized cell assemblies. Furthermore we observed similar coherence increases and spike phase shifts following DA application, suggesting a role for this neuromodulator, which is implicated in signaling reward expectation (Schultz et al., 1997). Activity synchronization may then lead to synaptic plasticity and the consolidation of assembly-related memory traces, as suggested by the enhanced replay of high-coherence related assemblies during post-training sleep.

Hpc-Pfc-θ Coherence Increases Further and Cell Assemblies Form at the Decision Point after Rule Acquisition

Theta band coherence between Hpc and Pfc has been shown previously (Siapas et al., 2005; Hyman et al., 2005) and linked with working memory (Jones and Wilson, 2005). The present data demonstrate that Hpc-Pfc-θ coherence augments at a critical part of the maze, where the rat has to commit to a potentially costly decision, based on a prediction of which arm is most likely to be rewarded. A reliable prediction is possible only when the rat has acquired the current task rule: indeed, coherence is maximally elevated only after the animal has reached criterion performance levels.

The increases in LFP coherence at the choice point and upon learning are accompanied by profound modifications of the dynamics of Pfc neural assemblies and local circuit dynamics. First, during high coherence, preferred firing phases shift, leading to Pfc cell assembly formation and firing in tight synchrony. These assemblies fire preferentially at the trough of Hpc theta and would hence be temporally aligned with hippocampal assemblies (Harris et al., 2003). This would enhance the impact of hippocampal inputs relative to those coming from other areas, influencing the formation of cell assemblies related to rule learning. After rule acquisition, this could also

have the effect of reinforcing this recently established network by increasing the probability that, within an assembly, the pre- and the postsynaptic spikes of two connected cells fall within a time interval suitable for triggering spike-timing dependent plasticity (STDP) (Markram et al., 1997; Bi and Poo, 1998; Buzsáki, 2004; Cassenaer and Laurent, 2007). Thus, this would facilitate consequent memory trace storage during sleep when these experience-related cell assemblies appearing during high Hpc-Pfc-θ-coherence are specifically replayed in transient bursts in concert with hippocampal sharp waves (Figure 8; also see Peyrache et al., 2009b).

Progressive Change of Phase of Pyramidal Neurons Leading up to Synchronization in Cell Assemblies

Pfc principal neurons' phase relative to Hpc theta changes progressively during high coherence to form synchronously firing cell assemblies. Experience-related modification of preferred phase relative to theta has been previously shown in hippocampus during REM sleep (Poe et al., 2000), as well as during active behavior (Hyman et al., 2005) and negative phase shifts (phase precession) toward the trough of Hpc theta were seen in some Pfc cells (Jones and Wilson, 2005). Here, the Pfc neurons taking part in CRCAs displayed a phase advance instead of precession (Figure 6). However, it is important to note that this pertains only to transient synchronization of small subsets of cells, which would not necessarily be detected by the population-wide, time-averaged analyses usually applied to study phase precession. In any case, both mechanisms would have the same effect, i.e., convergence of the firing phases toward the trough of Hpc theta.

Increased Local Inhibition during High Hpc-Pfc Theta Coherence

During high coherence, putative Pfc interneurons exercise more effective inhibitory control of principal cells. The importance of interneurons for generating and maintaining hippocampal theta oscillations is well documented (Buzsáki, 2002). Some interneurons, e.g., in the Hpc (Chapman and Lacaille, 1999), intrinsically oscillate at the theta rhythm, and interneurons are likely to support theta oscillations in the Pfc as well (Blatow et al., 2003). Pfc interneurons receive direct connections from the Hpc (Tierney et al., 2004) and thus it is not surprising that we observed that Pfc interneurons consistently remain phase locked to Hpc theta while putative pyramidal cells only follow theta during high Hpc-Pfc LFP coherence. Furthermore, interneurons can modify their activity in relation to external stimuli or to behavioral changes (Constantinidis and Goldman-Rakic, 2002; Monier et al., 2003; Fujisawa et al., 2008), and such changes may lead to the appearance and dissolution of cell assemblies (Geisler et al., 2007). Since interneuronal activity remains in phase with the peak of Hpc theta, an increase in inhibitory efficacy would constrain the pyramidal cells to fire primarily at a later phase (i.e., the trough) of the cycle, hence enforcing synchrony (Chapman and Lacaille, 1999). Therefore, the Pfc interneurons modulated by Hpc theta could act as a "latent theta oscillator," which is selectively enabled to control principal cell dynamics when behaviorally relevant information is processed, leading to the formation of cell assemblies.

Learning Related Changes in Hpc-Pfc Coherence, Inhibitory Efficacy and Theta Phase Locking in Pfc Resemble Effects of Dopamine Application

At the choice point and after learning, Hpc-Pfc coherence and inhibitory efficacy increase, Pfc neurons become synchronized to the Hpc theta trough and cell assemblies appear. The possible physiological mechanisms of the variations in synaptic efficacy enabling these events remain unknown, although neuromodulatory systems are presumed to play a role. Signals related to changes in reward anticipation (which would be expected as the rat chooses a goal arm) are broadcast in the brain via neuromodulatory signals such as DA (Schultz et al., 1997).

In our behavioral task, the choice point is likely to trigger reward expectation-dependent processes, possibly conveyed by DA. In a similar, multiple T-maze task, the ventral striatum displays a transient representation of expected reward (van der Meer and Redish, 2009) at the choice point. Accordingly, DA efflux in the Pfc has been shown to increase during the acquisition of a rule (van der Meulen et al., 2007). The increase in Hpc-Pfc theta coherence at the choice point would have the impact of heightening Pfc receptivity to Hpc signals as the rat evaluates the possible outcome of the two alternative choices. Indeed, the hippocampus (Johnson and Redish, 2007) generates representations of the two possible choice arms at the maze fork. We speculate that the Pfc, in concert with the striatum, participates in "parsing" these anticipated representations in terms of the predicted outcome of each choice. Reward expectation signals in the Pfc would be instrumental for this.

At the cellular level, activation of the D2 receptor can modulate the inhibitory effect of GABA-ergic interneurons on NMDA excitation of pyramidal cells (Tseng and O'Donnell, 2004). Moreover, DA in Pfc increases the reliability of interneurons' spike timing in response to Hpc stimulation (Tierney et al., 2008), and in vitro it increases IPSP amplitude and reduces spatiotemporal spread of stimulation-evoked activity (Bandyopadhyay and Hablitz, 2007). Finally, coapplication of dopamine and NMDA in slices was shown to induce neuronal synchronization nested within peaks in theta and gamma oscillations, a phenomenon that required activation of the dopamine D1 receptor (Gireesh and Plenz, 2008). The modification of the inhibitory synapses, and the consequent enforcement of precise spike timing over principal cells could thus explain both the increase in coherence and the formation of the cell assemblies observed in our experiments. Alternatively, the effect of DA could be due to a postsynaptic action on the slow potassic conductances of pyramidal neurons, which is known to affect the reliability of their response to an oscillatory input (Schreiber et al., 2004).

DA has powerful effects on synaptic plasticity as well: D1 agonists enhance LTP on Hpc-Pfc synapses (Gurden et al., 2000). In the hippocampus, dopamine affects STDP as well, by increasing induction sensitivity and expanding the temporal window for potentiation between pre- and postsynaptic spikes to at least 45 ms (Zhang et al., 2009). This enlarged window is compatible with the levels of temporal precision of our theta-synchronized assemblies in Pfc.

In anesthetized animals, we show that Pfc dopamine applications trigger the same pattern of changes observed in the maze when a reward prediction was required for making a choice. LFP

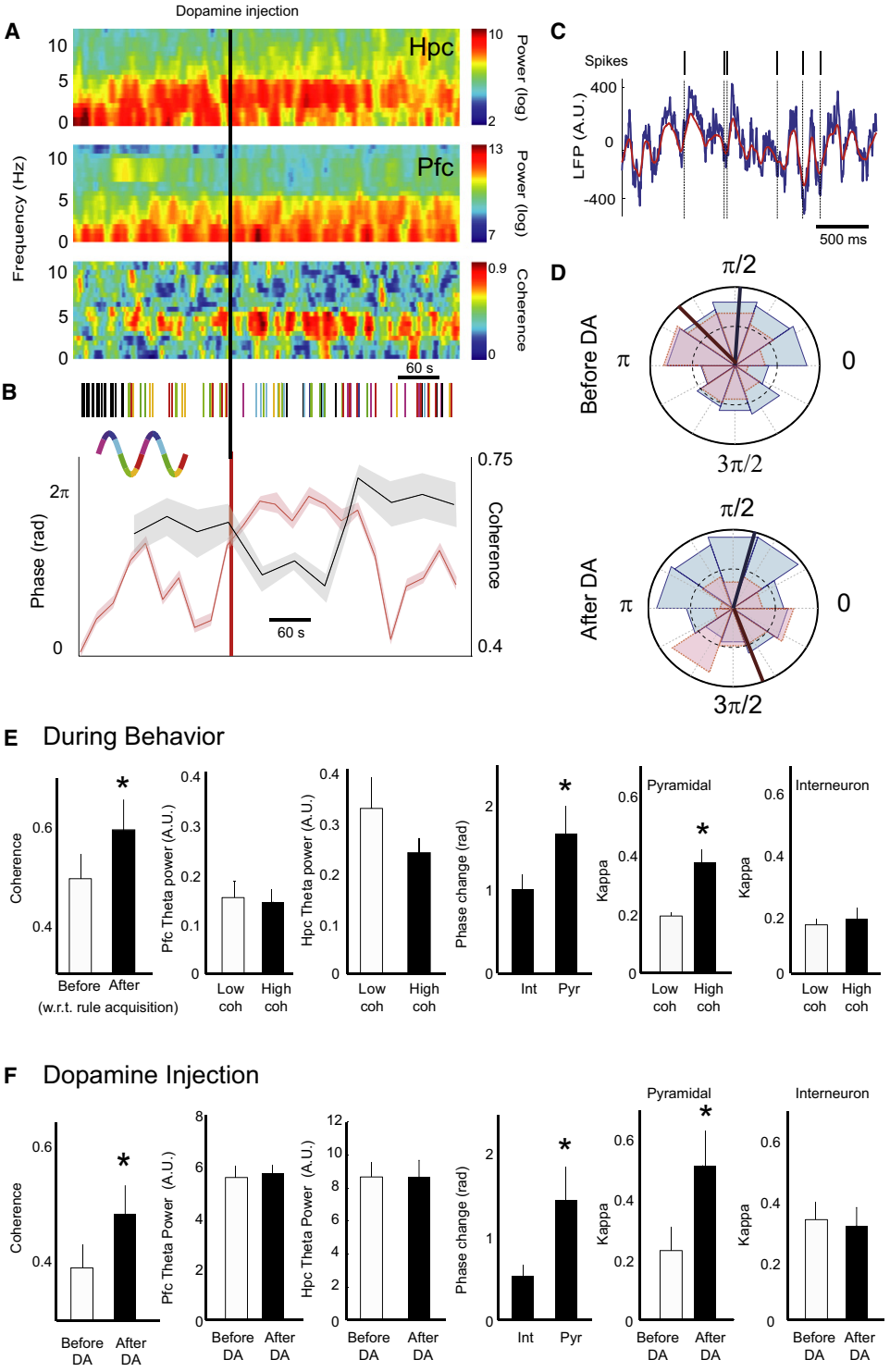

Figure 7. Local DA Injection Increases Coherence and Shifts Pfc Spike Phase Relative to Hpc Theta

(A) Following DA injection in Pfc of an anesthetized rat, Hpc (top) and Pfc (middle) spectrograms show little change in theta power while there is more coherence between Hpc and Pfc LFPs (bottom).

(B) Top, raster display of a Pfc pyramidal neuron before and after application of DA in Pfc. The phase of each spike with respect to Hpc theta is color coded (black: spikes in absence of theta). Bottom, mean phase (black curve) for these spikes and mean of coherence from (A) in the theta band (red curve). Note that spike phase changes after dopamine injection and then returns to the pre-injection value in concert with the coherence changes. Error bars: SEM computed over 1 min blocks of coherence readouts, each in a 1 s window.

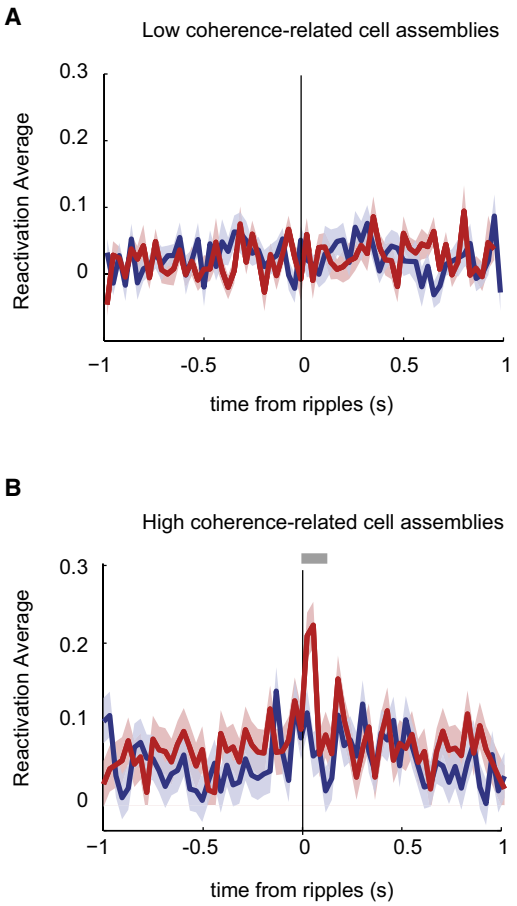

Figure 8. Reactivation of CRCA during Hippocampal Sharp Wave/Ripples (SPW-Rs)

PETH of average measure of temporal evolution of cell assembly coactivation computed during low coherence periods (A) or high coherence periods (B) relative to ripple timing obtained in sleep before (blue) and after the task performance/learning (red). Gray bars indicate significantly ($p < 0.05$, t test, $p < 0.05$, $n = 92$) higher reactivation strengths of cell assemblies with respect to baseline (defined as the average value from –1 to –0.5 s and from 0.5 to 1 s from the ripple timing). Error bars: SEM.

coherence between Hpc and Pfc theta increased, while theta power in the two structures is virtually unchanged. Pfc pyramidal cells shifted their theta phase preference to the Pfc theta trough under DA, while interneurons' preferred phase remained constant (Figure 7). While these data alone do not represent direct evidence, this striking parallel between anesthetized and behaving preparations is consistent with a role for phasic DA release in Pfc cell assembly formation at the decision point with learning. Taken together, these data suggest a possible mechanism linking together mechanisms at the network and cellular levels for reward signals to construct and "tag" activity configurations for long-term encoding: DA would increase assembly synchronization, making learning related assemblies to emerge, and then, because of the tight synchronization to be stabilized via STDP. Such mechanisms also may be applicable to understand DA mechanisms for learning in striatum. DA is not the only neuromodulator that might be involved in these processes. For example, in vitro acetylcholine both increases intrinsic theta oscillations in interneuronal networks (Blatow et al., 2003) and, through the nicotinic receptor, increases GABAergic inhibition of pyramidal cells (Couey et al., 2007).

These findings, taken together, point to a possible mechanism wherein coherence would help determine which information is stored in long-term memory. Thus, the Hpc/neocortical axis, deeply implicated in memory consolidation (Marr, 1970; Buzsáki, 1989; McClelland et al., 1995), may also be responsible during encoding, for the selection of the relevant information to be retained, possibly under neuromodulatory control.

EXPERIMENTAL PROCEDURES

Subjects, Surgical and Behavioral Protocols

Four Long-Evans male rats were pretrained to seek food reward on a Y maze under a regime of mild food deprivation. All experiments were in accord with institutional (CNRS Comité Opérationnel pour l'Ethique dans les Sciences de la Vie), international (NIH guidelines) standards and legal regulations (Certificat no. 7186, Ministère de l'Agriculture et de la Pêche) regarding the use and care of animals. Then they were implanted, under anesthesia, with a micro-drive containing six tetrodes above the right mPfc (AP 3.5–5 mm, ML 0.5–2 mm). A second micro-drive containing three tetrodes was placed above the right mid-ventral (AP −5.0 mm ML 5.0 mm). These latter tetrodes were used for LFP recordings. See Supplemental Experimental Procedures for more details.

Behavioral Protocols

Rats were trained in a rule-learning task involving attentional set shifts on a Y maze. Such extradimensional set shift tasks require an intact medial prefrontal cortex (Pfc) in rats (Birrell and Brown, 2000; Delatour and Gisquet-Verrier, 2000). This parallels the involvement of the human prefrontal cortex in the Wisconsin card-sorting task, which inspired the present experimental design. As explained in detail in Supplemental Experimental Procedures, at each trial, the rat had to choose one of two arms, the rewarded arm being either spatially guided to the left or the right or cue-guided to the illuminated or the dark arm. As soon as the rat acquired a rule, the reward contingency rule was changed, without any further signal, to a rule in the other stimulus dimension (i.e., from

(C) Example of Hpc LFP (blue: raw data, red: filtered in the theta band) and spikes of the same pyramidal cell as in (B).
(D) Preferred phase plots of a simultaneously recorded Pfc interneuron (blue) and pyramidal (red) cell pair, in Pfc before (top) and after (bottom) dopamine injection in Pfc. Preferred phase of the interneuron remains constant after injection (before injection: Rayleigh Z test, $p < 0.05$, $\phi_{pref} = 1.52$; after injection: Rayleigh Z test, $p < 0.05$, $\phi_{pref} = 1.43$, circular ANOVA, $p > 0.05$) while preferred phase of the pyramidal cell shifts to phase opposition relative to the interneuron after dopamine injection (before injection: Rayleigh Z test, $p < 0.05$, $\phi_{pref} = 2.44$; after injection: Rayleigh Z test, $p < 0.01$, $\phi_{pref} = 5.21$, circular ANOVA, $p < 0.05$).
(E and F) These panels compare properties in the behaving and anesthetized preparations. (E) From left to right: coherence before and after rule acquisition, theta power in Pfc and Hpc between high and low coherence, change of preferred phase between high and low coherence for interneurons and pyramidal cells, strength of Hpc theta modulation in Pfc pyramidal ($n = 6$) cells or interneurons ($n = 9$) with high PC weights during high and low coherence periods (t test, $^*p < 0.05$). (w.r.t.: with respect to; A.U.: arbitrary units.) (F) From left to right: coherence, theta power in Pfc and Hpc, preferred phase changes for interneurons and pyramidal cells, strength of Hpc theta modulation in Pfc pyramidal ($n = 6$) cells or interneurons ($n = 9$), before and after dopamine injection (t test, $^*p < 0.05$). Note that dopamine induced significant changes in coherence, preferred phase changes and Hpc theta modulation.
See also Figure S8.

spatially-guided to cue-guided, and vice versa). Because we were interested in the neural correlates of the early phases of task learning, rats were not exposed to the task until the first electrophysiological recording session. Each day, sleep sessions of 20–30 min were recorded before and after the maze task.

Electrophysiological Procedures

Signals from all electrodes were fed into a unity-gain headstage pre-amplifier (HS-54; Neuralynx, Bozeman, MT) and then, through a tether cable, to programmable amplifiers set at 2000x (Lynx-8, Neuralynx, Bozeman, MT). Signals for single unit recordings were band-pass filtered between 600 and 6000 Hz, signals for LFP recordings were filtered between 0.1 and 475 Hz (Pfc) and 1 and 475 Hz (Hpc). Data were digitized and stored on hard disk by the Power 1401 (CED, Cambridge, UK) acquisition system, controlled by Spike2 software (also by CED). Single unit data were sampled at 25 kHz, and 1.3 ms samples were time stamped and stored for all the channels in a tetrode whenever any of the 4 channels exceeded a pre-set threshold. Local field potentials were sampled and stored at 2 kHz.

Data Preprocessing

From spike waveforms, the energy (or squared averaged amplitude) and the first three principal components of the energy-normalized waveforms were computed for the four tetrode channels, generating a 12-dimensional vector describing each spike. Those vectors were input to the KlustaKwik (Harris et al., 2000) clustering program. The resulting classification was manually refined using the Klusters interface (Hazan et al., 2006).

Recording Sessions

Fifty-eight recording sessions were analyzed (Rat12, 12 days; Rat15, 19 days; Rat18, 14 days; Rat 19 13 days). A total of 1475 of putative single units were identified. All four rats learned the right and light rule. Because not all animals learned the remaining two rules and insufficient data were available, these were excluded from the analyses.

Identification of Putative Pyramidal Cells and Interneurons

Distribution of spike widths for all Pfc neurons recorded. According to previous studies (Barthó et al., 2004), putative interneurons and pyramidal cells in Pfc can be distinguished according to spike width. As previously described by Barthó and colleagues, the distribution of the spike width was bimodal (Figure S6). Cells with spike widths inferior to 0.3 ms were classified as putative interneurons (*blue zone*), whereas those superior to 0.35 ms (*vertical bars*) were classified as putative pyramidal cells (*pink zone*).

Coherence Analyses

Coherence and spectrograms were analyzed with multi-taper Fourier analysis (Mitra and Pesaran, 1999), making use of the Chronux toolbox (http://www.chronux.org), and with custom-written, MATLAB-based programs (MathWorks, Natick, MA). Coherence analyses concerned periods starting when the rat returned to the extremity of the start arm until it reached the reward site. The threshold for coherence to be considered as "high" was determined with the theoretical bound provided by the Chronux toolbox. A coherence of about 0.7 reached the statistical criterion ($p < 0.05$) and was then used as the threshold in the whole data set. Furthermore, since "low coherence" epochs were usually longer than "high coherence" ones, all analyses which aimed at comparing results between the two (correlation coefficient distributions, principal cells inhibition, etc.) were systematically controlled: statistics were carried out on randomly selected epochs from low coherence periods whose size (e.g., number of bins) were the same as the duration of high coherence epochs. Thus, the presented results were all independent from possible size effects.

Theta Modulation Analyses

The spike phase distribution relative to the theta oscillation is hypothesized to follow a Von Mises distribution (κ, concentration factor, a measure of phase dispersion; and ϕ_{pref}, preferred phase) (Fisher, 1993). Since the phase of theta depends on the recording site in Hpc, only recordings from electrodes in sessions where ripple oscillations were observed in the sleep periods before and after the task were included (ensuring recording in the CA1 pyramidal layer).

Principal Component Analysis

The method was based on that of (Peyrache et al., 2009a, 2009b) (Figure S5). (1) Spike trains from ensembles of simultaneously recorded Pfc cells were obtained from high coherence periods. (2) The spike trains were binned in 30 ms time windows (corresponding to the time window for Hpc cell assemblies [Harris et al., 2003]) or by theta cycle periods and then z transformed, so that each binned spike train had a zero mean and unit variance. (3) The correlation matrix of the z transformed binned spike trains was computed (an $N_{cells} \times N_{cells}$ matrix). (4) The principal components of the matrix were computed: the matrix is diagonalized, and the eigenvectors are sorted according to their associated eigenvalues. The eigenvectors corresponding to the three largest eigenvalues were termed "signal" components, while the others were considered "nonsignal," or noise. (5) Spike trains from ensembles of simultaneously recorded Pfc cells were obtained from the whole session. (6) The spike trains were binned in 30 ms time windows and then z transformed, leading to population vector of activity at any given time. (7) From each principal component, the dot product of the population vector with the projector of a principal component and then with the transposed population vector at any given time is computed, yielding the time course for the activation of that component referred as to "subnetworkcoactivation measure." Values that exceeded a threshold were taken to signify CRCA occurrence. For most analyses, we chose a threshold of 3, however different values of the threshold yielded similar results (Figure S5E).

Inhibitory Efficacy

Our method is derived from Constantinidis and colleagues (Constantinidis and Goldman-Rakic, 2002). For each interneuron within the CRCA, those putative pyramidal cells under its inhibitory influence were identified on the basis of (1) at least a 50% decrease in the number of spikes in the 5 ms after the interneuron's spike as compared to the 10 ms period before, and (2) no modification of the firing rate during high versus low coherence periods. Interneurons with small numbers of co-occurring pyramidal cells' spikes were excluded. All cross-correlograms were then normalized and averaged. The procedure was repeated for high and low coherence periods.

Pfc Recordings following Local Dopamine Infusions

Male Sprague-Dawley rats were placed in a stereotaxic apparatus under chloral hydrate anesthesia, maintained by intraperitoneal infusion of chloral hydrate with a peristaltic pump set at 60 mg/kg/hr turned on 1 hr after induction. Glass pipettes (20–30 MΩ) recorded extracellular unit activity in the PL/MO areas of the PFC (AP, +2.8–4 mm; ML, 0.4–1 mm; DV, 2.5–4 mm). DA was infused by iontophoresis through glass pipettes, initially with a current of 10 nA, which was increased in increments of 10–20 nA until an effect was observed.

Action potential duration was measured on the 2nd phase of the spike and the criteria for identification as an interneuron was that the action potential be inferior to 0.6 ms, as in Tierney et al. (2004). Coherence, preferred phase change, and theta modulation strength were compared between the five minutes before and after dopamine injection, but only when spontaneous theta activity was detected before the dopamine injection. Data from coherence and theta power were then averaged over all dopamine injections. All spikes before and after dopamine injection were pooled for the calculation of the preferred phase. Because DA has been shown to decrease neuronal firing rate in Pfc, spike analysis was performed when firing rate under dopamine injection remained at level over one half of that of the pre-DA injection period.

SUPPLEMENTAL INFORMATION

Supplemental Information includes eight figures and Supplemental Experimental Procedures and can be found with this article online at doi:10.1016/j.neuron.2010.05.013.

ACKNOWLEDGMENTS

We thank Prof. J.-M. Deniau, Drs. A.-M. Thierry and M.B. Zugaro for interesting discussions, S. Doutremer for histology, Prof. D. Hopkins and N. Quenech'du

for the anatomical reconstructions, V. Douchamps for help with the experiments, and Prof. A. Berthoz for support throughout the project. This work was supported by Fondation Fyssen (F.P.B.), Fondation pour la Recherche Medicale (A.P.), and EC contracts FP6-IST 027819 (ICEA), FP6-IST-027140 (BACS), and FP6-IST-027017 (NeuroProbes).

Accepted: May 11, 2010
Published: June 23, 2010

REFERENCES

Baeg, E.H., Kim, Y.B., Kim, J., Ghim, J.W., Kim, J.J., and Jung, M.W. (2007). Learning-induced enduring changes in functional connectivity among prefrontal cortical neurons. J. Neurosci. *27*, 909–918.

Bandyopadhyay, S., and Hablitz, J.J. (2007). Dopaminergic modulation of local network activity in rat prefrontal cortex. J. Neurophysiol. *97*, 4120–4128.

Barthó, P., Hirase, H., Monconduit, L., Zugaro, M., Harris, K.D., and Buzsáki, G. (2004). Characterization of neocortical principal cells and interneurons by network interactions and extracellular features. J. Neurophysiol. *92*, 600–608.

Bi, G.Q., and Poo, M.M. (1998). Synaptic modifications in cultured hippocampal neurons: dependence on spike timing, synaptic strength, and postsynaptic cell type. J. Neurosci. *18*, 10464–10472.

Birrell, J.M., and Brown, V.J. (2000). Medial frontal cortex mediates perceptual attentional set shifting in the rat. J. Neurosci. *20*, 4320–4324.

Blatow, M., Rozov, A., Katona, I., Hormuzdi, S.G., Meyer, A.H., Whittington, M.A., Caputi, A., and Monyer, H. (2003). A novel network of multipolar bursting interneurons generates theta frequency oscillations in neocortex. Neuron *38*, 805–817.

Buzsáki, G. (1989). Two-stage model of memory trace formation: a role for "noisy" brain states. Neuroscience *31*, 551–570.

Buzsáki, G. (2002). Theta oscillations in the hippocampus. Neuron *33*, 325–340.

Buzsáki, G. (2004). Large-scale recording of neuronal ensembles. Nat. Neurosci. *7*, 446–451.

Cassenaer, S., and Laurent, G. (2007). Hebbian STDP in mushroom bodies facilitates the synchronous flow of olfactory information in locusts. Nature *448*, 709–713.

Chapin, J.K., and Nicolelis, M.A. (1999). Principal component analysis of neuronal ensemble activity reveals multidimensional somatosensory representations. J. Neurosci. Methods *94*, 121–140.

Chapman, C.A., and Lacaille, J.C. (1999). Intrinsic theta-frequency membrane potential oscillations in hippocampal CA1 interneurons of stratum lacunosum-moleculare. J. Neurophysiol. *81*, 1296–1307.

Constantinidis, C., and Goldman-Rakic, P.S. (2002). Correlated discharges among putative pyramidal neurons and interneurons in the primate prefrontal cortex. J. Neurophysiol. *88*, 3487–3497.

Couey, J.J., Meredith, R.M., Spijker, S., Poorthuis, R.B., Smit, A.B., Brussaard, A.B., and Mansvelder, H.D. (2007). Distributed network actions by nicotine increase the threshold for spike-timing-dependent plasticity in prefrontal cortex. Neuron *54*, 73–87.

Dayan, P., and Balleine, B.W. (2002). Reward, motivation, and reinforcement learning. Neuron *36*, 285–298.

Dégenètais, E., Thierry, A.M., Glowinski, J., and Gioanni, Y. (2003). Synaptic influence of hippocampus on pyramidal cells of the rat prefrontal cortex: an in vivo intracellular recording study. Cereb. Cortex *13*, 782–792.

Delatour, B., and Gisquet-Verrier, P. (2000). Functional role of rat prelimbic-infralimbic cortices in spatial memory: evidence for their involvement in attention and behavioural flexibility. Behav. Brain Res. *109*, 113–128.

Doya, K. (2008). Modulators of decision making. Nat. Neurosci. *11*, 410–416.

Eichenbaum, H. (2000). A cortical-hippocampal system for declarative memory. Nat. Rev. Neurosci. *1*, 41–50.

Ekstrom, A.D., Meltzer, J., McNaughton, B.L., and Barnes, C.A. (2001). NMDA receptor antagonism blocks experience-dependent expansion of hippocampal "place fields". Neuron *31*, 631–638.

Engel, A.K., Fries, P., and Singer, W. (2001). Dynamic predictions: oscillations and synchrony in top-down processing. Nat. Rev. Neurosci. *2*, 704–716.

Fell, J., Klaver, P., Lehnertz, K., Grunwald, T., Schaller, C., Elger, C.E., and Fernández, G. (2001). Human memory formation is accompanied by rhinal-hippocampal coupling and decoupling. Nat. Neurosci. *4*, 1259–1264.

Felleman, D.J., and Van Essen, D.C. (1991). Distributed hierarchical processing in the primate cerebral cortex. Cereb. Cortex *1*, 1–47.

Fisher, N.I. (1993). Statistical Analysis of Circular Data (Cambridge: Cambridge University Press).

Floresco, S.B., Seamans, J.K., and Phillips, A.G. (1997). Selective roles for hippocampal, prefrontal cortical, and ventral striatal circuits in radial-arm maze tasks with or without a delay. J. Neurosci. *17*, 1880–1890.

Frankland, P.W., and Bontempi, B. (2005). The organization of recent and remote memories. Nat. Rev. Neurosci. *6*, 119–130.

Fries, P. (2005). A mechanism for cognitive dynamics: neuronal communication through neuronal coherence. Trends Cogn. Sci. *9*, 474–480.

Fries, P., Nikolić, D., and Singer, W. (2007). The gamma cycle. Trends Neurosci. *30*, 309–316.

Fujisawa, S., Amarasingham, A., Harrison, M.T., and Buzsáki, G. (2008). Behavior-dependent short-term assembly dynamics in the medial prefrontal cortex. Nat. Neurosci. *11*, 823–833.

Geisler, C., Robbe, D., Zugaro, M., Sirota, A., and Buzsáki, G. (2007). Hippocampal place cell assemblies are speed-controlled oscillators. Proc. Natl. Acad. Sci. USA *104*, 8149–8154.

Girardeau, G., Benchenane, K., Wiener, S.I., Buzsáki, G., and Zugaro, M.B. (2009). Selective suppression of hippocampal ripples impairs spatial memory. Nat. Neurosci. *12*, 1222–1223.

Gireesh, E.D., and Plenz, D. (2008). Neuronal avalanches organize as nested theta- and beta/gamma-oscillations during development of cortical layer 2/3. Proc. Natl. Acad. Sci. USA *105*, 7576–7581.

Gurden, H., Takita, M., and Jay, T.M. (2000). Essential role of D1 but not D2 receptors in the NMDA receptor-dependent long-term potentiation at hippocampal-prefrontal cortex synapses in vivo. J. Neurosci. *20*, RC106.

Harris, K.D., Henze, D.A., Csicsvari, J., Hirase, H., and Buzsáki, G. (2000). Accuracy of tetrode spike separation as determined by simultaneous intracellular and extracellular measurements. J. Neurophysiol. *84*, 401–414.

Harris, K.D., Csicsvari, J., Hirase, H., Dragoi, G., and Buzsáki, G. (2003). Organization of cell assemblies in the hippocampus. Nature *424*, 552–556.

Hazan, L., Zugaro, M., and Buzsáki, G. (2006). Klusters, NeuroScope, NDManager: a free software suite for neurophysiological data processing and visualization. J. Neurosci. Methods *155*, 207–216.

Hebb, D.O. (1949). The Organization of Behavior (New York: Wiley & Sons).

Hyman, J.M., Zilli, E.A., Paley, A.M., and Hasselmo, M.E. (2005). Medial prefrontal cortex cells show dynamic modulation with the hippocampal theta rhythm dependent on behavior. Hippocampus *15*, 739–749.

Jay, T.M., and Witter, M.P. (1991). Distribution of hippocampal CA1 and subicular efferents in the prefrontal cortex of the rat studied by means of anterograde transport of Phaseolus vulgaris-leucoagglutinin. J. Comp. Neurol. *313*, 574–586.

Johnson, A., and Redish, A.D. (2007). Neural ensembles in CA3 transiently encode paths forward of the animal at a decision point. J. Neurosci. *27*, 12176–12189.

Jones, M.W., and Wilson, M.A. (2005). Phase precession of medial prefrontal cortical activity relative to the hippocampal theta rhythm. Hippocampus *15*, 867–873.

Klausberger, T., Magill, P.J., Márton, L.F., Roberts, J.D., Cobden, P.M., Buzsáki, G., and Somogyi, P. (2003). Brain-state- and cell-type-specific firing of hippocampal interneurons in vivo. Nature *421*, 844–848.

Mann, E.O., and Paulsen, O. (2007). Role of GABAergic inhibition in hippocampal network oscillations. Trends Neurosci. *30*, 343–349.

Markram, H., Lübke, J., Frotscher, M., and Sakmann, B. (1997). Regulation of synaptic efficacy by coincidence of postsynaptic APs and EPSPs. Science *275*, 213–215.

Marr, D. (1970). A theory for cerebral neocortex. Proc. R. Soc. Lond. B Biol. Sci. *176*, 161–234.

McClelland, J.L., McNaughton, B.L., and O'Reilly, R.C. (1995). Why there are complementary learning systems in the hippocampus and neocortex: insights from the successes and failures of connectionist models of learning and memory. Psychol. Rev. *102*, 419–457.

Mitra, P.P., and Pesaran, B. (1999). Analysis of dynamic brain imaging data. Biophys. J. *76*, 691–708.

Monier, C., Chavane, F., Baudot, P., Graham, L.J., and Frégnac, Y. (2003). Orientation and direction selectivity of synaptic inputs in visual cortical neurons: a diversity of combinations produces spike tuning. Neuron *37*, 663–680.

Moscovitch, M., Rosenbaum, R.S., Gilboa, A., Addis, D.R., Westmacott, R., Grady, C., McAndrews, M.P., Levine, B., Black, S., Winocur, G., and Nadel, L. (2005). Functional neuroanatomy of remote episodic, semantic and spatial memory: a unified account based on multiple trace theory. J. Anat. *207*, 35–66.

Peyrache, A., Benchenane, K., Khamassi, M., Wiener, S.I., and Battaglia, F.P. (2009a). Principal component analysis of ensemble recordings reveals cell assemblies at high temporal resolution. J. Comput. Neurosci., in press. Published online June 16, 2009. 10.1007/s10827-009-0154-6.

Peyrache, A., Khamassi, M., Benchenane, K., Wiener, S.I., and Battaglia, F.P. (2009b). Replay of rule-learning related neural patterns in the prefrontal cortex during sleep. Nat. Neurosci. *12*, 919–926.

Poe, G.R., Nitz, D.A., McNaughton, B.L., and Barnes, C.A. (2000). Experience-dependent phase-reversal of hippocampal neuron firing during REM sleep. Brain Res. *855*, 176–180.

Schreiber, S., Fellous, J.M., Tiesinga, P., and Sejnowski, T.J. (2004). Influence of ionic conductances on spike timing reliability of cortical neurons for suprathreshold rhythmic inputs. J. Neurophysiol. *91*, 194–205.

Schultz, W., Dayan, P., and Montague, P.R. (1997). A neural substrate of prediction and reward. Science *275*, 1593–1599.

Shastri, L. (2002). Episodic memory and cortico-hippocampal interactions. Trends Cogn. Sci. *6*, 162–168.

Siapas, A.G., Lubenov, E.V., and Wilson, M.A. (2005). Prefrontal phase locking to hippocampal theta oscillations. Neuron *46*, 141–151.

Sirota, A., Montgomery, S., Fujisawa, S., Isomura, Y., Zugaro, M., and Buzsáki, G. (2008). Entrainment of neocortical neurons and gamma oscillations by the hippocampal theta rhythm. Neuron *60*, 683–697.

Smith, A.C., Frank, L.M., Wirth, S., Yanike, M., Hu, D., Kubota, Y., Graybiel, A.M., Suzuki, W.A., and Brown, E.N. (2004). Dynamic analysis of learning in behavioral experiments. J. Neurosci. *24*, 447–461.

Tabuchi, E.T., Mulder, A.B., and Wiener, S.I. (2000). Position and behavioral modulation of synchronization of hippocampal and accumbens neuronal discharges in freely moving rats. Hippocampus *10*, 717–728.

Thierry, A.M., Gioanni, Y., Dégénétais, E., and Glowinski, J. (2000). Hippocampo-prefrontal cortex pathway: anatomical and electrophysiological characteristics. Hippocampus *10*, 411–419.

Tierney, P.L., Dégenètais, E., Thierry, A.M., Glowinski, J., and Gioanni, Y. (2004). Influence of the hippocampus on interneurons of the rat prefrontal cortex. Eur. J. Neurosci. *20*, 514–524.

Tierney, P.L., Thierry, A.M., Glowinski, J., Deniau, J.M., and Gioanni, Y. (2008). Dopamine modulates temporal dynamics of feedforward inhibition in rat prefrontal cortex in vivo. Cereb. Cortex *18*, 2251–2262.

Tseng, K.Y., and O'Donnell, P. (2004). Dopamine-glutamate interactions controlling prefrontal cortical pyramidal cell excitability involve multiple signaling mechanisms. J. Neurosci. *24*, 5131–5139.

van der Meer, M.A., and Redish, A.D. (2009). Covert expectation-of-reward in rat ventral striatum at decision points. Front. Integr. Neurosci. *3*, 9.

van der Meulen, J.A., Joosten, R.N., de Bruin, J.P., and Feenstra, M.G. (2007). Dopamine and noradrenaline efflux in the medial prefrontal cortex during serial reversals and extinction of instrumental goal-directed behavior. Cereb. Cortex *17*, 1444–1453.

Varela, F., Lachaux, J.P., Rodriguez, E., and Martinerie, J. (2001). The brainweb: phase synchronization and large-scale integration. Nat. Rev. Neurosci. *2*, 229–239.

Womelsdorf, T., Schoffelen, J.M., Oostenveld, R., Singer, W., Desimone, R., Engel, A.K., and Fries, P. (2007). Modulation of neuronal interactions through neuronal synchronization. Science *316*, 1609–1612.

Zhang, J.C., Lau, P.M., and Bi, G.Q. (2009). Gain in sensitivity and loss in temporal contrast of STDP by dopaminergic modulation at hippocampal synapses. Proc. Natl. Acad. Sci. USA *106*, 13028–13033.

Article

Coherent Theta Oscillations and Reorganization of Spike Timing in the Hippocampal-Prefrontal Network upon Learning

Karim Benchenane, Adrien Peyrache, Mehdi Khamassi, Patrick Tierney, Yves Gioanni, Francesco P. Battaglia, Sidney I. Wiener

Supplemental Figure Legends and Experimental Procedures.

Figure S1. (related to Figure 1)

A) *Left*, Cresyl violet stained 60 μm sections with an electrolytic lesion at the recording site in the Hpc. *Right*, reconstructed tracks of recording tetrodes in Pfc for one rat.

B-D) Sorted spike waveform data from one example tetrode recording (displays adapted from the Klusters program, see Methods). B) Scatter plots of two projections representing first principal component (PC) for the four channels for each spike. Differently colored points denote spikes assigned to the eight cells. C) Example waveforms from the respective tetrode wires, with same color code as in (B). D) Auto-correlograms (in color) and cross-correlograms (gray) for the 8 cells (timescale: -30 to +30 ms).

E-F) To control for potential contamination of LFP coherence measures by volume conduction artifacts, we compared LFP-LFP coherence with LFP-spikes coherence in the same structures. E) Correlation between the time series for Hpc-Pfc LFPs spectral coherence (*ordinate*) and the coherence between Hpc LFP and spikes of all Hpc theta modulated Pfc neurons in the same session (n=13 out of 39 recorded neurons, Rayleigh test $p<0.05$) pooled as multi-unit activity (*abscissa*) as a function of frequency. F) Statistical significance of panel E. Note that, at the LFP level, coherence is only moderately correlated with prefrontal theta power ($r=0.34$ for the session showing the largest effect) and hippocampal power ($r=0.25$)

(not shown). This moderate correlation could be due to the increased likelihood of registering larger coherence readouts when the signal to noise ratio for these phases is higher. When data points with very weak theta (theta/delta ratio<2) are eliminated, the correlations are markedly smaller (with Pfc power: r = 0.15, p = 0.03, with Hpc power: r = 0.04, n.s.).

Figure S2. (related to Figure 2)

A) In the Y maze, the liquid rewards were first at the right arm independent of which arm was lit. (Left and right arms were lit in a pseudo-random sequence). In the subsequent cue-guided task the reward was at the lit arm, independent of whether it was at the left or right position.

B) Average number of days necessary for acquisition for these two rules (Right and Light, n=4; mean±SEM).

C) Coherence between electrodes in hippocampus and prefrontal layers 2/3 or layer 5 at the decision point is higher after rule acquisition (Right and Light). (Two-way ANOVA, main effect of learning, $p<0.01$, main effect of electrode localization $p<0.05$, interaction $p>0.05$.)

D) Average of Hpc-Pfc theta coherence before (gray) and after (black) rule acquisition, and of movement velocity before (blue) and after (red) rule acquisition (n= 542 trials, over 21 sessions). *Abscissa*: distance that the rat traversed on the Y-maze from the extremity of the start arm to the reward site. Error bars: SEM.

E) Average of Hpc-Pfc theta coherence before (gray) and after (black) rule acquisition (as in D but with ordinate shifted), and of movement acceleration before (blue) and after (red) rule acquisition (n= 542 trials, over 21 sessions). *Abscissa*: Same as in (D).

F-G) Correlation between mean values of coherence and speed (F) and acceleration (G) depicted in panels D and E respectively. Note that for positive values of acceleration, coherence was still higher after learning (same color code as in D and E). Correlations

between coherence and acceleration or speed at the decision point for each trial are not significant (speed: r=0.04, p>0.05 and acceleration r=0.01, p>0.05).

H-I) Average of Hpc-Pfc theta coherence (H) and acceleration (I) after rule acquisition (n= 226 trials) when rats went to the reward site (*forward*, in red) and when they returned to the departure arm (*back*, black). *Abscissa*: distance that the rat traversed on the Y-maze from the extremity of the start arm to the reward site. Shaded area: SEM. Note that during the return trip, coherence stayed almost constant, despite that the rats first accelerated and then decelerated strongly.

Figure S3. (related to Figure 3)

A) The firing rate of 45 simultaneously recorded neurons during periods of low and high Hpc-Pfc theta coherence were computed for 30 ms bins over the recording session, and then used to compute correlation matrices. The resulting significantly correlated neuron pairs are connected by lines. Blue points represent neurons modulated by hippocampal theta. More pairs are co-activated in high coherence periods after rule acquisition. These pairs are primarily composed of Hpc theta modulated neurons (cf., Fig. 3C). Note that significant correlations are observed in neurons from different tetrodes (indicated by arcs of different colors).

B) Distribution of coefficients of the correlation matrix of all neurons recorded simultaneously in a single representative session, binned in 30 ms time windows (*left column*), or by theta cycle (*right column*) taken from high coherence periods (*red trace*) or from low coherence periods (*blue filled area*). The distributions are significantly different, Kolmogorov-Smirnov-test, p<0.05. Since the durations of high and low coherence periods are different, to compare distributions of correlation coefficients, two approaches were used: either by randomly taking the same number of bins in low coherence periods as in high

coherence periods or by normalizing the coefficient correlation by the square root of the number of bins in each period. In both cases, the distributions of correlation coefficients were significantly different (Kolmogorov-Smirnov test, $p<0.05$)

C,D) Proportion of pairs of neurons with significant correlations among (from left to right) all pairs of non-theta modulated cells, among pairs consisting of a theta-modulated and a non-modulated cell, or pairs of theta-modulated cells, computed for high and low theta coherence (coh) periods. Spike trains are binned in 30 ms (left) or theta cycle (right) time windows. Analysis are from all sessions (B, n=60), or those with rule acquisition (C, n=35). The proportion of pairs of theta modulated neurons is greater during high coherence epochs for both methods (*stars*, t-test, $p<0.01$, number of neurons recorded simultaneously: min: 7, max: 55).

E) Same analysis as C and D in sessions with rule acquisition, separated into trials before and after rule acquisition for theta-modulated cell pairs only. Spike trains are binned in 30 ms (*left*) or theta cycle (*right*) time windows. Same color code as in C; n=5 sessions, two-way ANOVA, post-hoc t-test, $p<0.05$ for both)

Figure S4. (related to Figure 4)

A) Raster display of 31 simultaneously recorded neurons ordered from top to bottom according to their weights in the first PC in this session. *Below)* Temporal evolution of subnetwork coactivation (*black trace*) superimposed on the concurrent coherence spectrogram. Note that the peak in subnetwork coactivation corresponds to synchronous firing of neurons with high absolute weights in the PC (*red star above*). Note the looser synchronization of the cell assembly when Hpc-Pfc theta coherence is reduced (*black star*). Such events yield only small bumps in thel evolution of subnetwork coactivation trace.

The signs of the PC weights distinguish two neuronal populations: cells with same signed PC weights fire together (*orange shaded zone*), whereas cells with opposite signed coefficients are anti-correlated (*blue shaded zone*). Cells with the highest PC weights (in absolute value) were those that made the strongest contribution to the subnetwork activation. Mathematically, peaks of the subnetwork activation measure could be due to alternate co-firing of the two groups (with respectively high positive and negative PC weights). However, practically, peaks of the subnetwork reactivation measure are always due to the co-firing of the same group, the second remaining silent at those times. Since, the sign obtained with the PCA is undetermined, the PC weight of co-firing neurons was arbitrarily chosen as positive.

Visual inspection of rasters of the whole data set reveals that in every case, at least five neurons fired together during peaks of the subnetwork activation measure. The cells with the five highest weights in the PC were thus considered as composing the CRCA. In Figure 5, neurons with the five highest and the five lowest PC weights (high absolute PC weights) were considered since all had a strong influence on cell assembly formation.

B) *Above*, Raster display of 23 simultaneously recorded neurons ordered from top to bottom according to their weights in the first PC in this session. *Below*, Only highly synchronous firing leads to a network coactivation values (R) above the threshold value of 3.

C) Distribution of network coactivation values for one representative session. The threshold value of 3 represents the 95th percentile of the distribution.

D) Same plot as C on pooled data from 3 different sessions in log/log scale. The red line represents linear regression, showing that the tail of the distribution of the network coactivation values follow a power law (see Peyrache et al., 2009a,b).

E) Phase of CRCA remains stable relative to hippocampal theta, with CRCA defined by three different thresholds (*left*, threshold=1, n=207, κ=0.19, p=0.15, φpref=0.78; *middle*,

threshold=3, n=51, κ=0.66, p=0.005, φpref=1.08; *right*, threshold=5, n=37, κ=0.74, p=0.009, φpref= 0.99).

Figure S5. (related to Figure 4)

A) PCA of spike trains binned in 30 ms time windows or by theta cycles leads to the identification of the same cell assemblies. Four representative sessions showing that in both cases CRCAs are modulated by theta and have the same preferred phase. Moreover, PC weights of neurons obtained with the two bin widths are highly correlated.

B) The same analyses as Figure 4D were performed with PCs corresponding to 'noise' or 'non-signal' (*i.e.* low PC eigenvalues, see Peyrache et al., 2009a,b) related to high coherence periods (*top row*), and for cell assemblies with high eigenvalues but calculated from low coherence periods (*bottom row*) as controls. In each case, all preferred phases were uniformly distributed throughout the theta cycle (n=70 for noise PC, and n=72 for cell assemblies related to low coherence periods, Rayleigh Z-test, $p>0.05$), with no modification during high versus low coherence periods (circular ANOVA, $p>0.05$).

Figure S6. (related to Figure 5)

A) Distribution of spike widths for all Pfc neurons recorded. Cells with spike widths inferior to 0.3 ms were classified as putative interneurons (*blue zone*) whereas those superior to 0.35 ms (*vertical bars*) were classified as putative pyramidal cells (*pink zone*) (Bartho et al., 2004).

B) The four zones analyzed in the Y-maze (for trajectories from the departure arm to the reward sites only).

C) Cross-correlograms between eight simultaneously recorded interneurons and pyramidal cell pairs with high absolute PC weights in the decision point zone, before and after rule

acquisition. Averages over the eight interneurons' cross-correlograms appear beneath, showing significantly greater inhibition after rule acquisition (paired t-test before [-5, 0 ms] and after [0, 5 ms], * - $p<0.0001$). Gray scale shows normalized firing rates as z-scores.

Figure S7. (related to Figure 6)

The same analysis as in Fig. 6B with the same number of CRCA activations used as reference, but chosen at random times during high coherence periods. Note that the phases of the neuronal population remained fixed at the trough of theta (the preferred phase of pyramidal neurons; see Fig. 5A) without modification of phase, suggesting that the modification of phase seen before CRCA activation is specific to cell assembly formation rather than simply a general phase procession/precession process as previously described in Pfc (Jones et al., 2005a).

Figure S8. (related to Figure 7)

Identification of putative Pfc pyramidal cells and interneurons in acute experiments with local DA administration. Sorted spike waveforms from one example recording (displays adapted from Klusters, see Methods). A) Example waveforms from two discriminated cells (interneuron in blue, pyramidal cell in red). B) Scatter plots of two projections representing first PC scores for each spike. Points of different colors denote spikes assigned to the two cells, color code as in A. C, D) Auto-correlograms for the two cells at different time scales.

Supplemental Experimental procedures

Subjects

Four pigmented Long-Evans male rats (René Janvier, Le Genest-St-Isle, France) weighing 250-300g at arrival, were kept on a 12h on/12h off light schedule (lights on at 8am) in an approved animal facility. Pre-training and experiments were performed during the lights-on period. Rats were permitted to habituate to the colony room for at least two weeks before the beginning of pre-training; in that period they were regularly handled by the experimenters. Rats were housed in pairs until the beginning of pre-training, then singly housed for the duration of the experiment. From the start of the pre-training, rats were on a mild food-deprivation regime (14 g rat chow daily). All experiments were in accord with institutional (CNRS Comité Opérationnel pour l'Ethique dans les Sciences de la Vie), international (NIH guidelines) standards and legal regulations (Certicat no. 7186, Ministère de l'Agriculture et de la Pêche) regarding the use and care of animals.

Surgical procedures

For at least a week before surgery, rats were habituated to running on the maze where the behavioral task took place by allowing them to forage on the maze for 5-25 minutes daily, with reward available at the end of the arms.

For surgery, rats were anesthetized with intra-muscular Xylazine (Rompun 0.1 ml), followed by intra-peritoneal pentobarbital (35 mg/kg) with supplements of the latter as necessary. An assembly containing 6-8 independently drivable tetrodes was implanted on the skull above the right medial prefrontal cortex (AP 3.5-5 mm, ML 0.5-2 mm). Each tetrode was inserted in 30 gauge hypodermic tubing, with the tubes soldered together in two parallel adjacent rows. Tetrodes (Gray et al., 1995) were twisted bundles of 13 μm diameter polyimide-coated nichrome wire (Kanthal, Palm Coast, FL). Individual microdrives allowed independent adjustment of tetrode depths. After dura retraction, the cannulae assembly was implanted

parallel and adjacent to the sagittal sinus, so that they targeted, respectively, the superficial and deep layers of the medial bank of the cortex. A separate micro-drive containing three tetrodes was targeted to mid-ventral hippocampal CA1 (AP -5.0 mm, ML 5.0 mm). Each of these tetrodes was electrically connected in a single-electrode configuration (all channels shorted together) and used for local field potential (LFP) recordings. For all LFP recordings, a screw implanted in the occipital bone above the cerebellum was used as a reference. After surgery, rats were allowed to recover for at least 2 weeks, while the tetrodes were gradually lowered to reach the prefrontal cortical prelimbic area and the CA1 pyramidal layer, respectively.

Behavioral protocols

Each recording session consisted of a 20-30 minutes sleep, or rest, epoch in which the rat was allowed to remain undisturbed in a padded flowerpot placed on the central platform of the maze. This was followed by an 'awake' epoch, in which the rat performed the behavioral task (described below) for 20-40 minutes, followed by a second sleep or rest epoch of 20-30 minutes. The first recording sessions corresponded to the first time rats encountered reward contingencies. Rats started each trial in the same 'departure' arm with the central barrier in place. One of the two other (goal) arms was illuminated at random (pseudo-random schedule: runs of more than 4 consecutive trials with the same illuminated arm were avoided as were extended runs of alternation). After that, the barrier to the central platform was removed, allowing the rat to access the goal arms. Only one of the goal arms was rewarded according to one of four rules. Two rules were spatially guided (always go to the right arm, or to the left arm), the other two were cue guided (go to the illuminated arm, or to the dark arm). The current rule was not signaled in any way, so that the animal had to determine the rule by trial and error. Once the rat reached a criterion of 10 consecutive correct trials, or only one error out of 12 trials, the rule was changed with no further cue warning to the rat. Rule changes

were extra-dimensional, that is, from a spatially-guided rule to a cue-guided rule, and vice versa. The software used for analysing behavioral performance (certainty measure) is a modified version of software downloaded from Anne Smith's homepage (http://neurostat.mgh.harvard.edu/BehavioralLearning/Matlabcode) (Smith et al., 2004).

Histology

At the end of the experiments, small electrolytic lesions were made by passing a small cathodal DC current (20 μA, 10 s) through each recording tetrode to mark the location of its tip. The rats were then deeply anesthetized with pentobarbital. Intracardial perfusion with saline was followed by 10% formalin saline. Histological sections were stained with cresyl violet.

Pfc recordings following local dopamine infusions

The detailed protocol was described before (Tierney et al., 2008). Briefly, male Sprague-Dawley rats (Charles River, L'Arbresle, France) weighing 280-350 g were placed in a stereotaxic apparatus (Unimécanique, Asnières, France) after anesthesia induction with a 400-mg/kg intraperitoneal injection of chloral hydrate. Anesthesia maintenance was ensured by intraperitoneal infusion of chloral hydrate with a peristaltic pump set at 60 mg/kg/h turned on 1 h after induction. Proper depth of anesthesia was assessed regularly by testing the limb withdrawal reflex and monitoring of cortical activity for signs of arousal. Glass pipettes (20-30 MΩ) recorded extracellular unit activity in the PL/MO areas of the PFC (AP: + 2.8-4 mm from bregma; ML: 0.4-1 mm; depth: 2.5-4 mm from the cortical surface. For the iontophoresis experiments, 5-barrel glass pipettes (Harvard Apparatus, Kent, UK) were used (10-40 MΩ). Under microscopic control the glass recording pipette was glued 15-30 microns below the tip of the 5-barrel iontophoresis pipette. Five high impedance current control units (Bionic Instruments, Bris-sur-Forges, France) were used to deliver currents for the

iontophoresis experiments. Retention currents were set at 8-10 nA. Ejection currents were adjusted for each cell. In brief, DA was initially iontophoresed with a current of 10 nA and increased in increments of 10-20 nA until an effect was observed.

Action potential duration was measured on the 2nd phase of the spike and the criteria for identification as an interneuron was that the action potential be inferior to 0.6 ms, as in Tierney et al (2004). Coherence, preferred phase change and theta modulation strength were compared between the five minutes before and after dopamine injection, but only when spontaneous theta activity was detected before the dopamine injection. Data from coherence and theta power were then averaged over all dopamine injections. All spikes before and after dopamine injection were pooled for the calculation of the preferred phase. Because DA has been shown to decrease neuronal firing rate in Pfc, spike analysis was performed when firing rate under dopamine injection remained at level over one half of that of the pre-dopamine injection period.

Pfc recordings following local dopamine infusions

The detailed protocol was described before (Tierney, 2008). Briefly, male Sprague-Dawley rats (Charles River, L'Arbresle, France) weighing 280-350 g were placed in a stereotaxic apparatus (Unimécanique, Asnières, France) after anesthesia induction with a 400-mg/kg intraperitoneal injection of chloral hydrate. Anesthesia maintenance was ensured by intraperitoneal infusion of chloral hydrate with a peristaltic pump set at 60 mg/kg/h turned on 1 h after induction. Proper depth of anesthesia was assessed regularly by testing the limb withdrawal reflex and monitoring of cortical activity for signs of arousal. Glass pipettes (20-30 MΩ) recorded extracellular unit activity in the PL/MO areas of the PFC (AP: + 2.8-4 mm from bregma; ML: 0.4-1 mm; depth: 2.5-4 mm from the cortical surface. For the iontophoresis experiments, 5-barrel glass pipettes (Harvard Apparatus, Kent, UK) were used (10-40 MΩ). Under microscopic control the glass recording pipette was glued 15-30 microns

below the tip of the 5-barrel iontophoresis pipette. Five high impedance current control units (Bionic Instruments, Bris-sur-Forges, France) were used to deliver currents for the iontophoresis experiments. Retention currents were set at 8-10 nA. Ejection currents were adjusted for each cell. In brief, DA was initially iontophoresed with a current of 10 nA and increased in increments of 10-20 nA until an effect was observed.

Action potential duration was measured on the 2nd phase of the spike and the criteria for identification as an interneuron was that the action potential be inferior to 0.6 ms, as in Tierney et al. (2004). Coherence, preferred phase change and theta modulation strength were compared between the five minutes before and after dopamine injection, but only when spontaneous theta activity was detected before the dopamine injection. Data from coherence and theta power were then averaged over all dopamine injections. All spikes before and after dopamine injection were pooled for the calculation of the preferred phase. Because DA has been shown to decrease neuronal firing rate in Pfc, spike analysis was performed when firing rate under dopamine injection remained at level over one half of that of the pre-dopamine injection period.

A

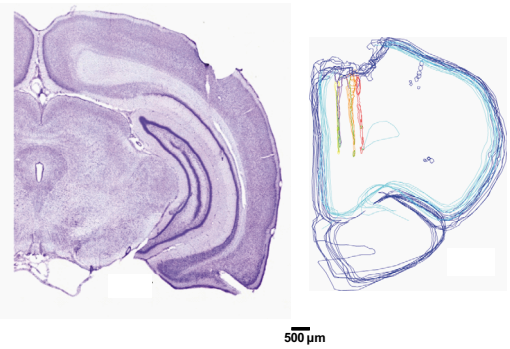
500 µm

B

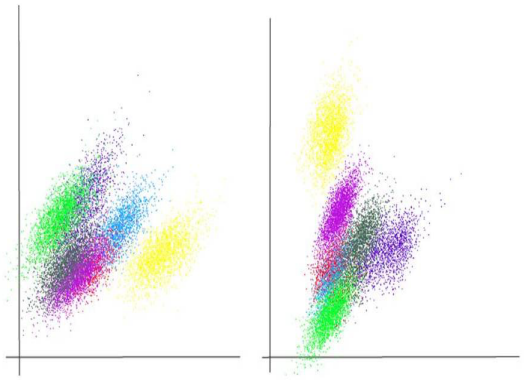

C

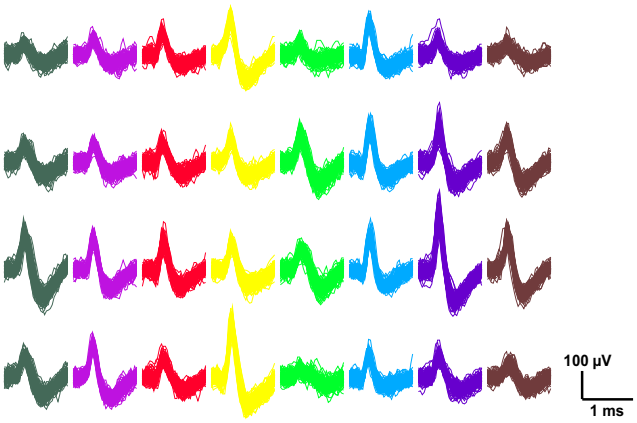
100 µV
1 ms

D

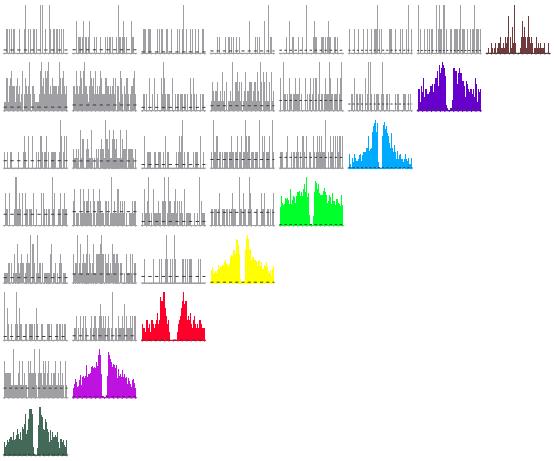

E

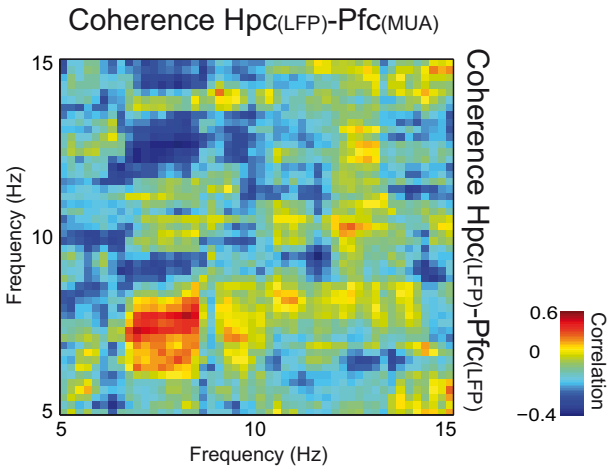
Coherence Hpc(LFP)-Pfc(MUA)
Frequency (Hz)
Frequency (Hz)
Coherence Hpc(LFP)-Pfc(LFP)
Correlation
0.6
0
−0.4
15
10
5

F

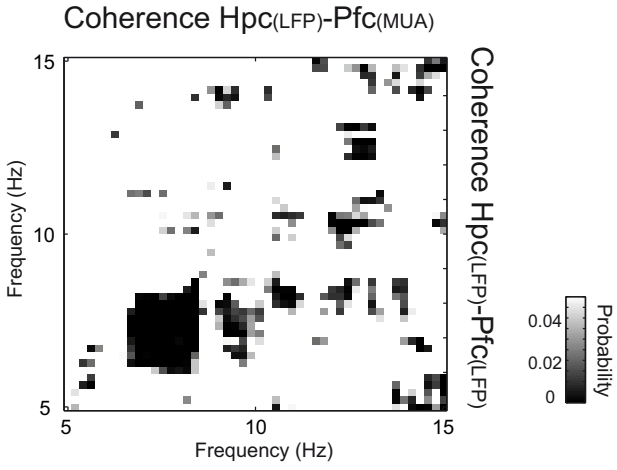
Coherence Hpc(LFP)-Pfc(MUA)
Frequency (Hz)
Frequency (Hz)
Coherence Hpc(LFP)-Pfc(LFP)
Probability
0.04
0.02
0
15
10
5

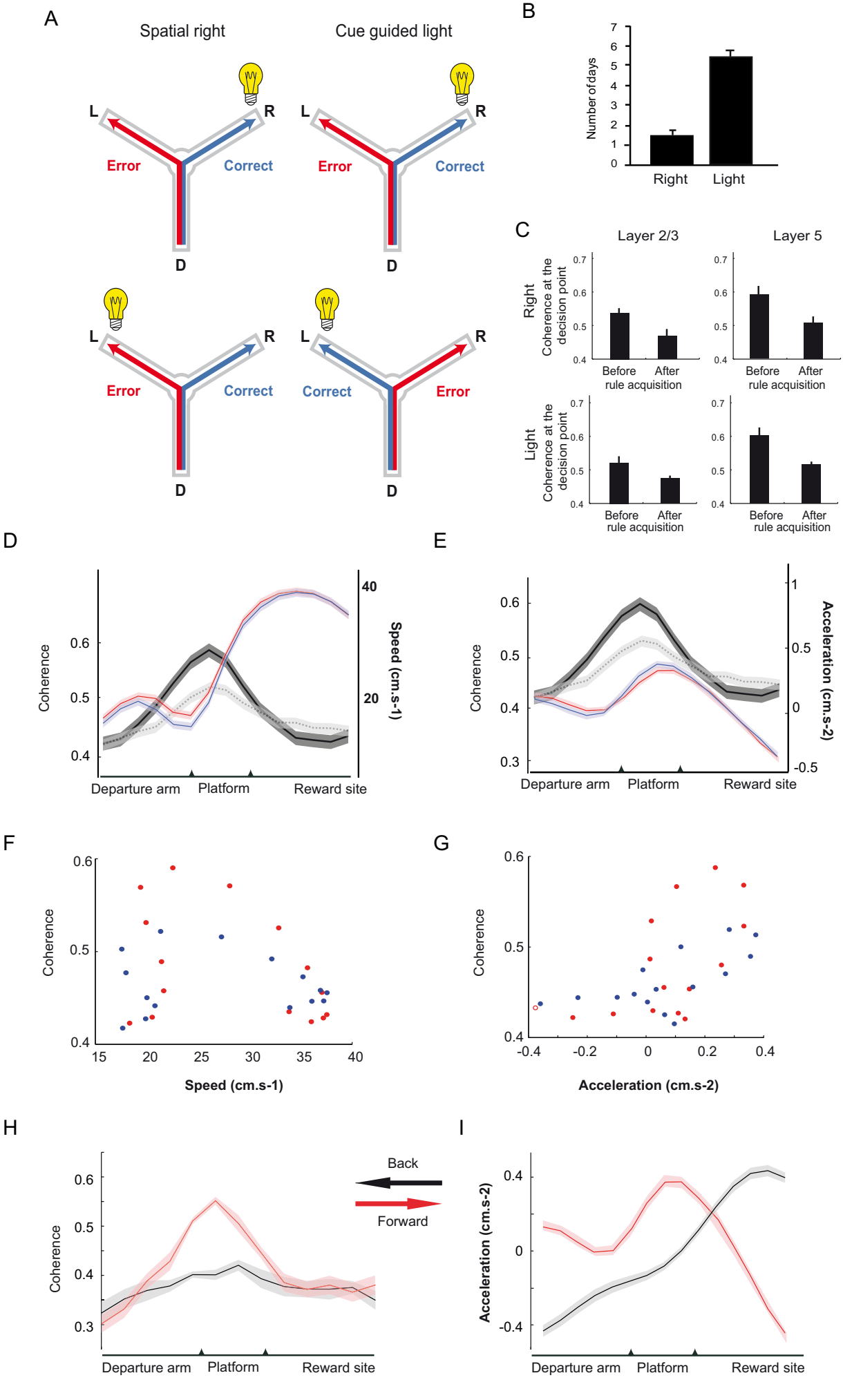
A
Spatial right
Cue guided light
L
R
Error
Correct
D
B
Number of days
Right
Light
C
Layer 2/3
Layer 5
Right
Light
Coherence at the decision point
Before rule acquisition
After rule acquisition
D
Coherence
Speed (cm.s-1)
Departure arm
Platform
Reward site
E
Acceleration (cm.s-2)
F
Speed (cm.s-1)
G
Acceleration (cm.s-2)
H
Back
Forward
I

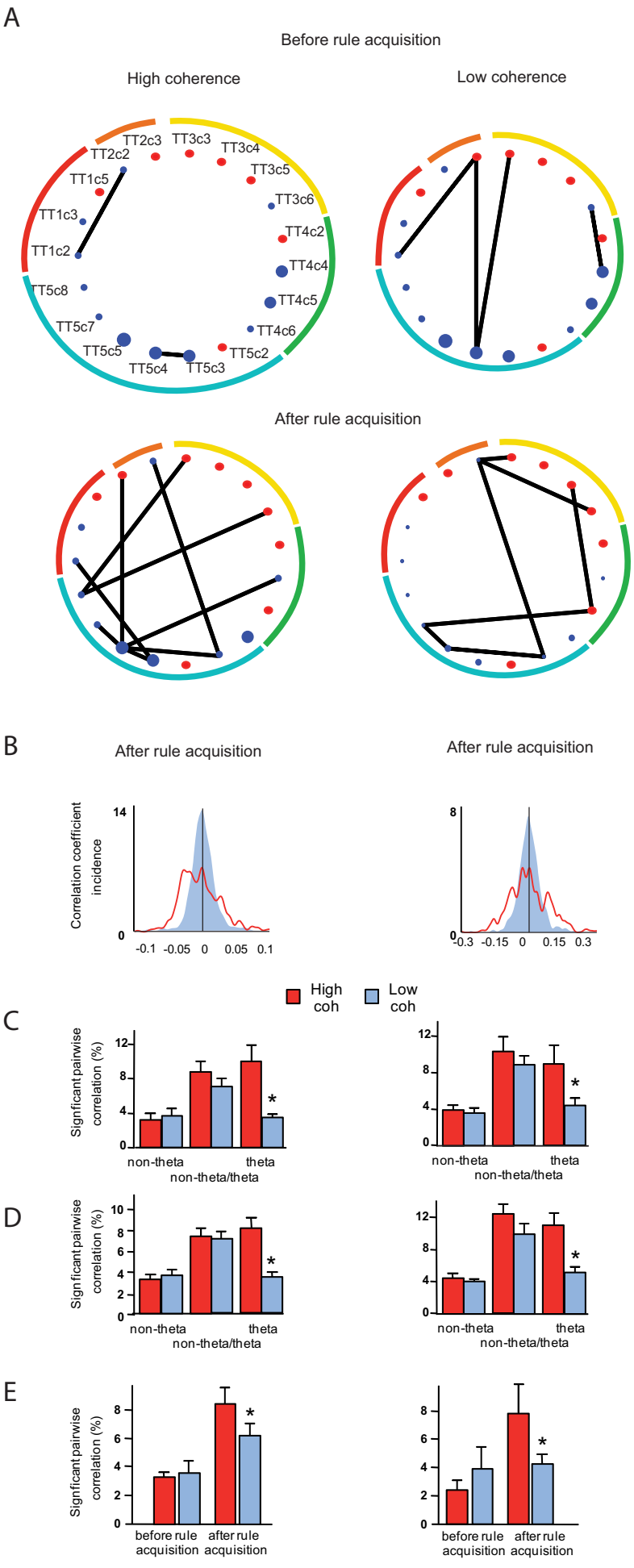
A
Before rule acquisition
High coherence
Low coherence
TT2c3
TT3c3
TT3c4
TT2c2
TT3c5
TT1c5
TT3c6
TT1c3
TT4c2
TT1c2
TT4c4
TT5c8
TT4c5
TT5c7
TT4c6
TT5c5
TT5c2
TT5c4
TT5c3
After rule acquisition
B
After rule acquisition
After rule acquisition
Correlation coefficient incidence
14
0
-0.1 -0.05 0 0.05 0.1
8
0
-0.3 -0.15 0 0.15 0.3
High coh
Low coh
C
Signficant pairwise correlation (%)
12
8
4
0
non-theta
theta
non-theta/theta
*
D
Signficant pairwise correlation (%)
10
8
6
4
2
0
E
Signficant pairwise correlation (%)
before rule acquisition
after rule acquisition

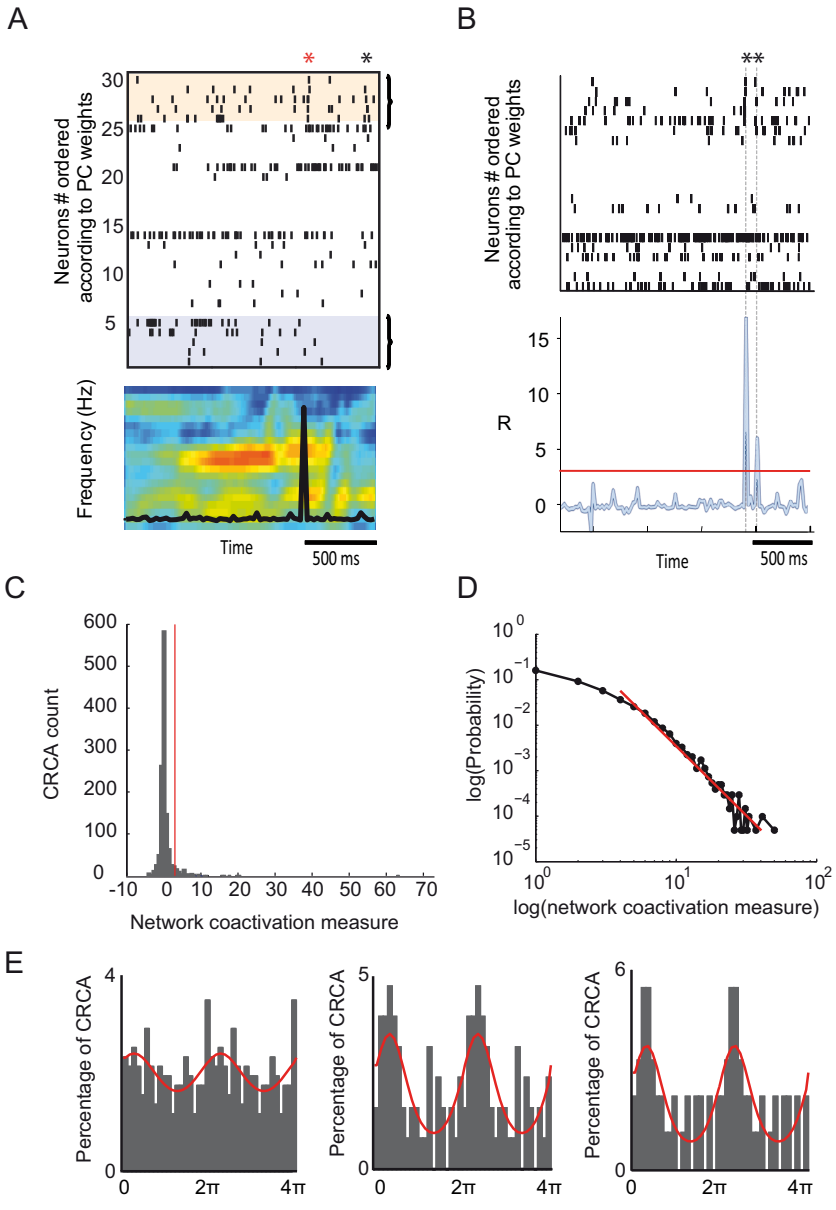
A
B
C
D
E
Neurons # ordered according to PC weights
Frequency (Hz)
Time
500 ms
R
CRCA count
Network coactivation measure
log(Probability)
log(network coactivation measure)
Percentage of CRCA
0
2π
4π

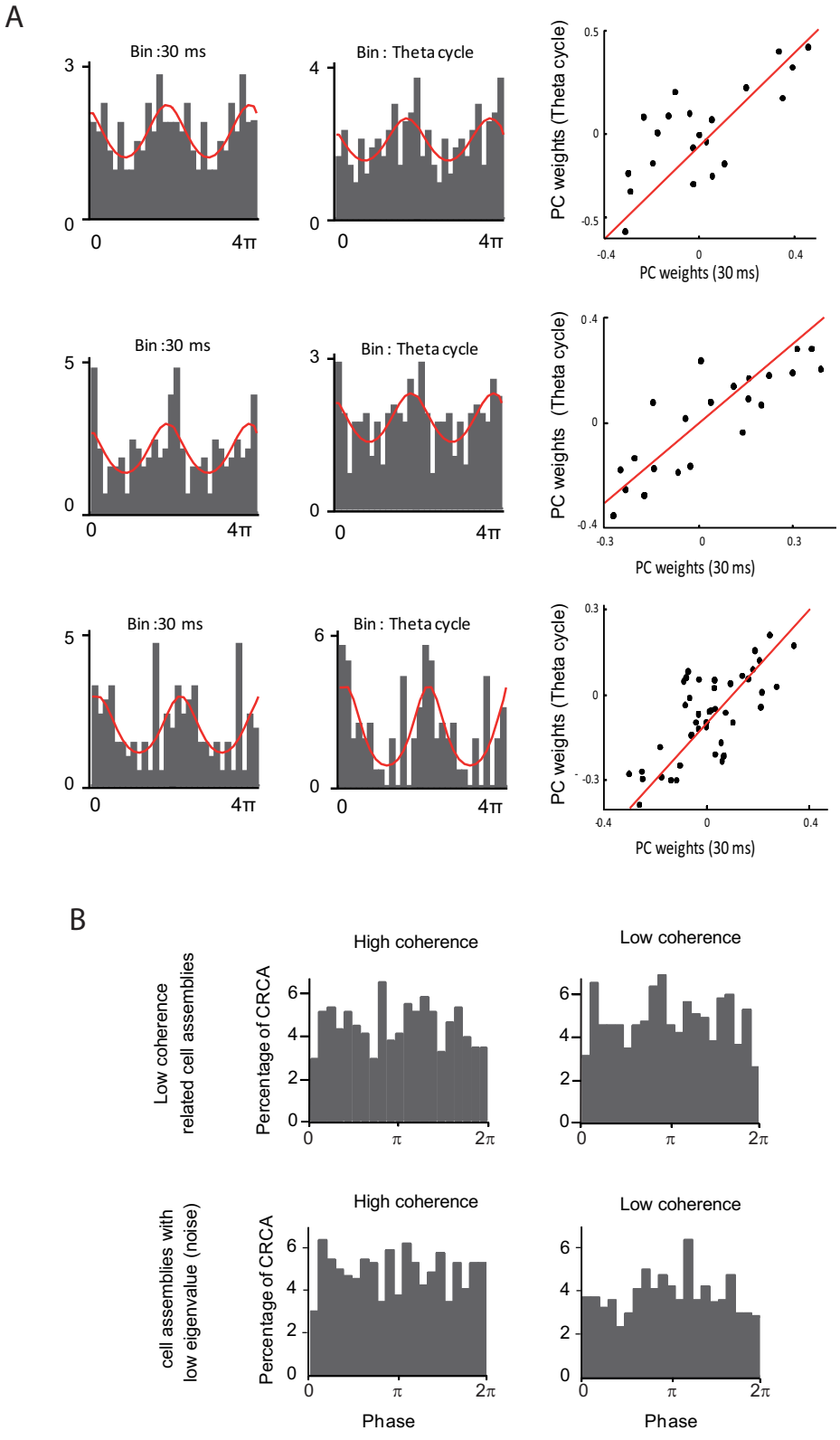
A
Bin :30 ms
Bin : Theta cycle
PC weights (Theta cycle)
PC weights (30 ms)
B
High coherence
Low coherence
Low coherence related cell assemblies
cell assemblies with low eigenvalue (noise)
Percentage of CRCA
Phase

A

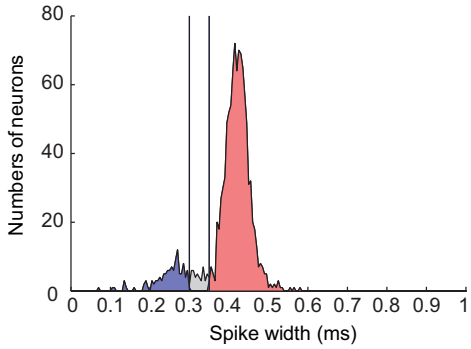
Numbers of neurons
80
60
40
20
0
0 0.1 0.2 0.3 0.4 0.5 0.6 0.7 0.8 0.9 1
Spike width (ms)

B

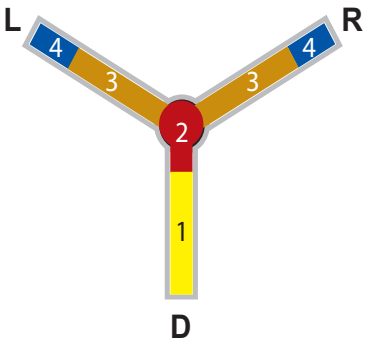
L
R
4
3
3
4
2
1
D

C

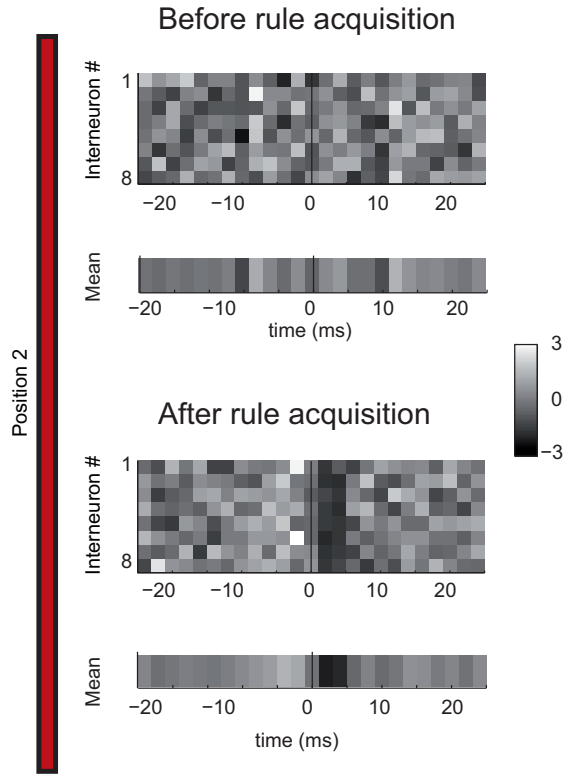
Before rule acquisition
Interneuron #
1
8
−20 −10 0 10 20
Mean
−20 −10 0 10 20
time (ms)
3
0
−3
After rule acquisition
Interneuron #
1
8
−20 −10 0 10 20
Mean
−20 −10 0 10 20
time (ms)
Position 2

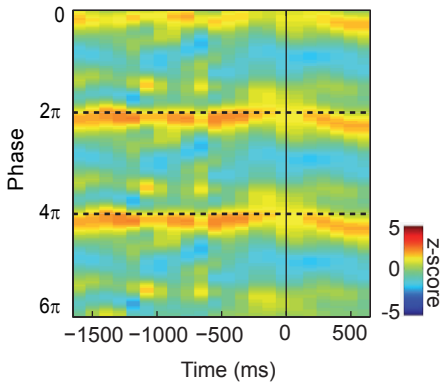
0
2π
4π
6π
Phase
−1500 −1000 −500 0 500
Time (ms)
5
0
-5
z-score

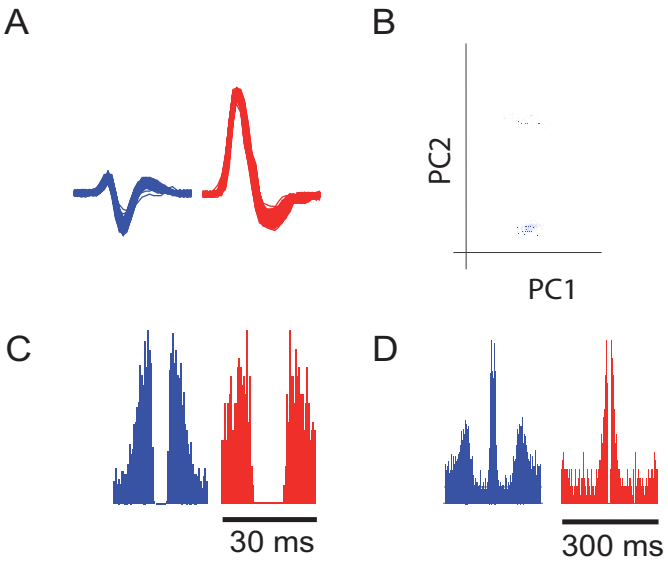
A
B
PC2
PC1
C
30 ms
D
300 ms